

ORIGINAL RESEARCH

PVECs-Derived Exosomal microRNAs Regulate PSMCs via FoxM1 Signaling in IUGR-induced Pulmonary Hypertension

Xiaofei Luo , PhD; Chengcheng Hang , PhD; Ziming Zhang , PhD; Kaixing Le , MS; Yuhan Ying , MS; Ying Lv , PhD; Lingling Yan , PhD; Yajie Huang , PhD; Lixia Ye , PhD; Xuefeng Xu , PhD; Ying Zhong , PhD; Lizhong Du , PhD

BACKGROUND: Intrauterine growth restriction (IUGR) is closely related to systemic or pulmonary hypertension (PH) in adulthood. Aberrant crosstalk between pulmonary vascular endothelial cells (PVECs) and pulmonary arterial smooth muscle cells (PASCs) that is mediated by exosomes plays an essential role in the progression of PH. FoxM1 (Forkhead box M1) is a key transcription factor that governs many important biological processes.

METHODS AND RESULTS: IUGR-induced PH rat models were established. Transwell plates were used to coculture PVECs and PASCs. Exosomes were isolated from PVEC-derived medium, and a microRNA (miRNA) screening was proceeded to identify effects of IUGR on small RNAs enclosed within exosomes. Dual-Luciferase assay was performed to validate the predicted binding sites of miRNAs on FoxM1 3' untranslated region. FoxM1 inhibitor thiothrepton was used in IUGR-induced PH rats. In this study, we found that FoxM1 expression was remarkably increased in IUGR-induced PH, and PASCs were regulated by PVECs through FoxM1 signaling in a non-contact way. An miRNA screening showed that miR-214-3p, miR-326-3p, and miR-125b-2-3p were downregulated in PVEC-derived exosomes of the IUGR group, which were associated with overexpression of FoxM1 and more significant proliferation and migration of PASCs. Dual-Luciferase assay demonstrated that the 3 miRNAs directly targeted FoxM1 3' untranslated region. FoxM1 inhibition blocked the PVECs-PASCs crosstalk and reversed the abnormal functions of PASCs. In vivo, treatment with thiothrepton significantly reduced the severity of PH.

CONCLUSIONS: Transmission of exosomal miRNAs from PVECs regulated the functions of PASCs via FoxM1 signaling, and FoxM1 may serve as a potential therapeutic target in IUGR-induced PH.

Key Words: exosomal microRNAs ■ Forkhead box M1 ■ intercellular communication ■ intrauterine growth restriction ■ pulmonary hypertension

The “Developmental Origins of Health and Disease” suggests that harmful exposures during early life increase the risk of disease later in life.¹ Intrauterine growth restriction (IUGR) is generally defined as an estimated fetal weight below the 10th percentile for gestational age and sex that may be caused by maternal, placental, fetal, or genetic factors.² Despite its multiple origins, IUGR is associated with higher risks of

cardiovascular diseases, including systemic or pulmonary hypertension (PH).^{3,4} PH is a complex pathology characterized by abnormal vascular remodeling and a progressive rise in the pulmonary vascular load, leading to hypertrophy and remodeling of the right ventricle.⁵ A large prospective single-site study found that about 18% of extremely low-birth-weight infants were likely to develop PH.⁶ Another study found that a transient perinatal

Correspondence to: Lizhong Du, PhD, The Children's Hospital, Zhejiang University School of Medicine, No. 3333 Binsheng Rd, Hangzhou, Zhejiang Province 310052, People's Republic of China. Email: dulizhong@zju.edu.cn

*X. Luo and C. Hang contributed equally.

Supplemental Material is available at <https://www.ahajournals.org/doi/suppl/10.1161/JAHA.122.027177>

For Sources of Funding and Disclosures, see page 13.

© 2022 The Authors. Published on behalf of the American Heart Association, Inc., by Wiley. This is an open access article under the terms of the [Creative Commons Attribution-NonCommercial-NoDerivs](https://creativecommons.org/licenses/by-nc-nd/4.0/) License, which permits use and distribution in any medium, provided the original work is properly cited, the use is non-commercial and no modifications or adaptations are made.

JAHA is available at: www.ahajournals.org/journal/jaha

CLINICAL PERSPECTIVE

What Is New?

- We provided direct evidence that pulmonary vascular endothelial cells could regulate the proliferation and migration of pulmonary arterial smooth muscle cells through FoxM1 (Forkhead box M1) signaling in intrauterine growth restriction (IUGR)-induced pulmonary hypertension.
- We uncovered that IUGR could change the microRNA cargos enclosed within exosomes to mediate the intercellular communication that is potentially relevant to pulmonary hypertension that occurs following IUGR.

What Are the Clinical Implications?

- MiR-214-3p, miR-326-3p, and miR-125b-2-3p may be triggers for the induction of exaggerated pulmonary hypertension in IUGR and served as biomarkers for this disease.
- FoxM1 inhibition might provide a novel therapeutic approach to ameliorate the effects of IUGR on exaggerated pulmonary hypertension.

Nonstandard Abbreviations and Acronyms

ECs	endothelial cells
EdU	5-ethynyl-2'-deoxyuridine
FBS	fetal bovine serum
FoxM1	Forkhead box M1
IUGR	intrauterine growth restriction
miRNAs	microRNAs
mPAP	mean pulmonary arterial pressure
PASMCs	pulmonary arterial smooth muscle cells
PH	pulmonary hypertension
PVECs	pulmonary vascular endothelial cells
SMCs	smooth muscle cells
UTR	untranslated region

insult to the pulmonary circulation left a persistent and potentially fatal imprint that may evoke the development of PH in adult life.⁷ However, the mechanism under PH that occurs following IUGR is poorly documented.

Pulmonary vascular endothelial cells (PVECs) and pulmonary arterial smooth muscle cells (PASMCs) are 2 key cell types that play major roles in the structural remodeling process of the pulmonary vasculature. Endothelial injury or dysfunction has been believed to be the initial event.⁸ Smooth muscle cells (SMCs) are the predominant cells of vessels, whose hypertrophy, proliferation, and migration may result in obstruction of the vascular lumen, causing elevations in

mean pulmonary arterial pressure (mPAP).⁹ Studies on the pathogenesis of PH highlighted the intercellular communication between vascular cells, especially endothelial cells (ECs) and SMCs. Prior works demonstrated that ECs can regulate the functions of underlying SMCs through cocultured SMCs with EC-derived medium.^{10,11} In addition to such paracrine regulation, other intercellular communication via the myoendothelial junctions and extracellular vesicles also plays an important role in the pathobiology of PH.¹² Because of the complex signalings involved in the process of PH, identification of the critical molecular mechanism mediating vascular cell hyperproliferation and migration is vital to develop strategies to potentially reverse the PH.

Among the mechanisms evaluated, FoxM1 (Forkhead box M1) is a key transcription factor of cell cycle progression that is required for G1/S and G2/M transition, as well as the M-phase progression.^{13,14} Studies found that FoxM1 is a central downstream effector on which various pro-proliferative and inflammatory stimuli converge.^{15–17} FoxM1 promoted pulmonary vascular development by directly stimulating proliferation of developing SMCs, and constitutive deletion of SMC FoxM1 in mice induced arterial wall defects and premature death immediately after birth.¹⁵ However, whether the PH risk induced by IUGR is coupled with FoxM1, and the role of FoxM1 in the crosstalk between PVECs and PASMCs, remains undefined.

Exosomes are small vesicles (traditionally considered 50–150 nm in diameter) that can be secreted by almost all cell types.¹⁸ Exosomes have been recognized as potent vehicles of intercellular communication that can influence physiological and pathological functions of the recipient cells.¹⁹ MicroRNAs (miRNAs) are endogenous 21–23 nt small noncoding RNAs, which are proposed to regulate over one-half of all human genes, finetuning a diverse array of biological processes.²⁰ Secreted miRNAs enclosed within exosomes can be protected from degradation by ribonuclease, functioning as stable diagnostic biomarkers or therapeutic targets.²¹ Various kinds of miRNAs were reported to specifically affect vascular cells and contribute to the pathogenesis of PH.²² Therefore, it is crucial to recognize the major mechanism underlying miRNA functions in IUGR-induced PH.

In the current study, we established an IUGR rat model of PH to verify the effect of adverse intrauterine environment in later life. We hypothesized that aberrant crosstalk between PVECs and PASMCs, which was mediated by exosomal miRNAs through FoxM1 signaling, played an essential role in the pathology of IUGR-induced PH, and FoxM1 inhibition might provide an effective solution for such multifactorial disease. This study described a novel, microRNA-dependent association between PVECs and PASMCs and suggested

a novel mechanism to ameliorate the effects of IUGR on exaggerated PH.

METHODS

We have full access to all the data in the study and take responsibility for their integrity and the data analysis. The data that support the findings of this study are available from the corresponding author upon reasonable request.

Ethics Statement of Animal Studies

The animal care and study protocols were approved by the Institutional Animal Care and Use Committee of Zhejiang University. All experiments were performed in accordance with the National Institutes of Health guidelines. Sprague–Dawley Rats were used for experimental data with the minimum of suffering. Wild-type rats were purchased from Zhejiang Chinese Medical University Laboratory Animal Center.

Rat Model Establishment

We used a rodent model of nutrient restriction during pregnancy to induce IUGR in offspring as described in our previous study.^{23,24} Pups of food-restricted mothers, weighing <10th percentile of the controls, were considered as the IUGR group.² Only male pups were studied to avoid hormonal cycle disturbances.^{25,26} Offspring rats at 9 weeks were exposed to hypoxia with 10% oxygen concentration for 3 weeks to induce PH. Then offspring rats were randomly allocated to receive the FoxM1 inhibitor thioestrepton (10 mg/kg, Aladdin, China) or its vehicle intraperitoneally every day for 3 weeks.¹⁷

Primary PVECs and PASMCs Culture

Rat primary PVECs were harvested as described in our previous studies.²⁴ PVECs were cultured in EC media supplemented with 5% fetal bovine serum (FBS), 1% EC growth supplement, and 1% antibiotics (all from Science Cell, USA). Heparin (yuanye, China) was added at 90 U/mL to inhibit the growth of fibroblasts and purify ECs. The cells were authenticated by specific cell marker CD31, and the purity was over 90% (Figure S1A). PVECs were used between passages 1 and 2.

Rat PASMCs were cultured from peripheral small pulmonary artery using an enzymatic dissociation method as our previous description.²⁷ DMEM high glucose containing 15% FBS and 1% antibiotics (all from Gibco, USA) were used to culture PASMCs, and experiments were performed with PASMCs from passages 2 to 4. Cells were positively stained for specific α -smooth muscle actin by immunofluorescence, and the purity was >90% (Figure S1B).

Coculture System of PVECs and PASMCs

A noncontact coculture system of PVECs and PASMCs was developed through a transwell system (Figure S1C). Briefly, PVECs were seeded on the upper sides of 0.4- μ m pore cell culture inserts (Corning, USA), while PASMCs were seeded on the matched culture plates. PVECs and PASMCs were cultured in their respective complete media overnight to fully attach, and then the inserts were put into the plates and maintained in the system in DMEM supplemented with 2% FBS for 48 hours at 37 °C.^{28,29}

Preparation of PVEC-Derived Medium

1×10^6 of primary PVECs in exponential growth period were cultured in a 15-cm plate overnight to adhere. Then the media was discarded and cells washed with PBS to remove residual FBS. PVECs continued to culture for 48 hours with 5 mL of EC media without any supplement, such as FBS, EC growth supplement, antibiotics, and heparin. Then the culture media was pipetted and centrifuged at 2000g for 30 minutes. The supernatant was collected and used as PVEC-derived medium.

Exosomal miRNAs Isolation, Sequencing, and Differential Expression Analysis

PVEC-derived medium from 8 plates was pooled for exosomes isolation. The isolated particles were characterized by transmission electron microscope studies, nanoparticle tracking analysis, and Western blot analysis of exosome markers CD63, TSG101, and HSP70. The differential exosomal miRNA expression analysis was performed after sequencing on an Illumina HiSeq platform.

Statistical Analysis

Statistical analysis was performed with Student *t*-test for comparisons between 2 groups. One-way ANOVA was performed for comparison of >2 groups, followed by Dunnett test compared with their corresponding controls or Tukey test. Welch ANOVA followed by Games-Howell multiple comparison was performed if the equal variance of data was not assumed. Two-way ANOVA was performed for comparisons with 2 variables, followed by Bonferroni multiple comparison test to analysis the effects of IUGR or hypoxia. All statistical analyses were performed using Prism8.3.0 (La Jolla, CA) and SPSS 22.0 (SPSS, Inc). Data were represented as mean \pm SEM. Comparisons were considered statistically significant when the *P* value was <0.05. Duplicated experiments were performed independently to guarantee reproducibility of findings.

Detailed methods are provided in Data S1. Additionally, all research listed in the Methods is included in the Major Resources Table and provided as Table S1.

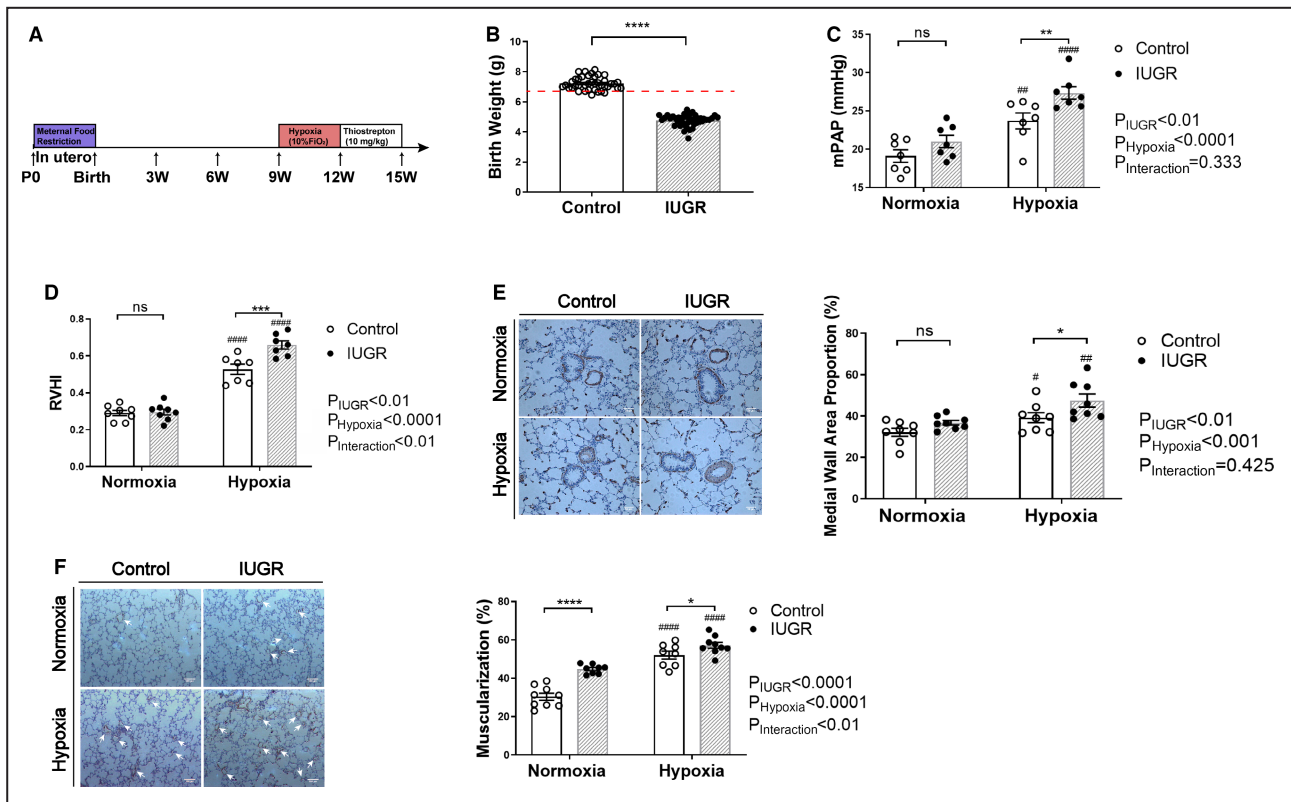


Figure 1. Intrauterine growth restriction-induced pulmonary hypertension rat models were established.

A, Intrauterine growth restriction-induced pulmonary hypertension rat model design and treatment. **B**, Birth weight (g) of intrauterine growth restriction ($n=42$) and control ($n=40$) rats. The red dotted line indicates the 10th percentile of the controls' birth weight. **C**, Mean pulmonary arterial pressure of the rats ($n=7$ per group). **D**, Right ventricular hypertrophy index of the rats (=right ventricular weight/[left ventricular weight plus septum weight]) ($n=7-8$ per group). **E**, Representative images of lung tissue stained with α -smooth muscle actin and medial wall area proportion of pulmonary arteriole, which is $<100\ \mu\text{m}$ in diameter. Medial wall area proportion=(outer area-inner area)/outer area ($n=8$ per group). Scale bar= $50\ \mu\text{m}$. **F**, Representative images of α -smooth muscle actin staining and muscularization of distal pulmonary vessels, which is $<100\ \mu\text{m}$ in diameter ($n=8-9$ per group). Scale bar= $100\ \mu\text{m}$. All data were represented as the mean \pm SEM. Comparisons of birth weights were made using Student *t*-test; comparisons in **C** through **F** were made using 2-way ANOVA. IUGR indicates intrauterine growth restriction; and RVHI, right ventricular hypertrophy index. * $P<0.05$, ** $P<0.01$, *** $P<0.001$, **** $P<0.0001$, comparison between intrauterine growth restriction and control groups as indicated; # $P<0.05$, ## $P<0.01$, ### $P<0.0001$, comparison with relative group under normoxia.

RESULTS

IUGR-Induced PH Rat Models Were Established

IUGR-induced PH rat models were designed as shown in Figure 1A. IUGR pups developed significantly lower birth

weights than controls, with all pups' birth weights falling below the 10th percentile of the controls, which meant that the IUGR rat models had been successfully established (Figure 1B). Both IUGR and hypoxia increased the mPAP (Figure 1C), the right ventricular (RV) hypertrophy index (Figure 1D), the medial wall thickness of vascular

Figure 2. FoxM1 expression was remarkably increased in intrauterine growth restriction-induced pulmonary hypertension.

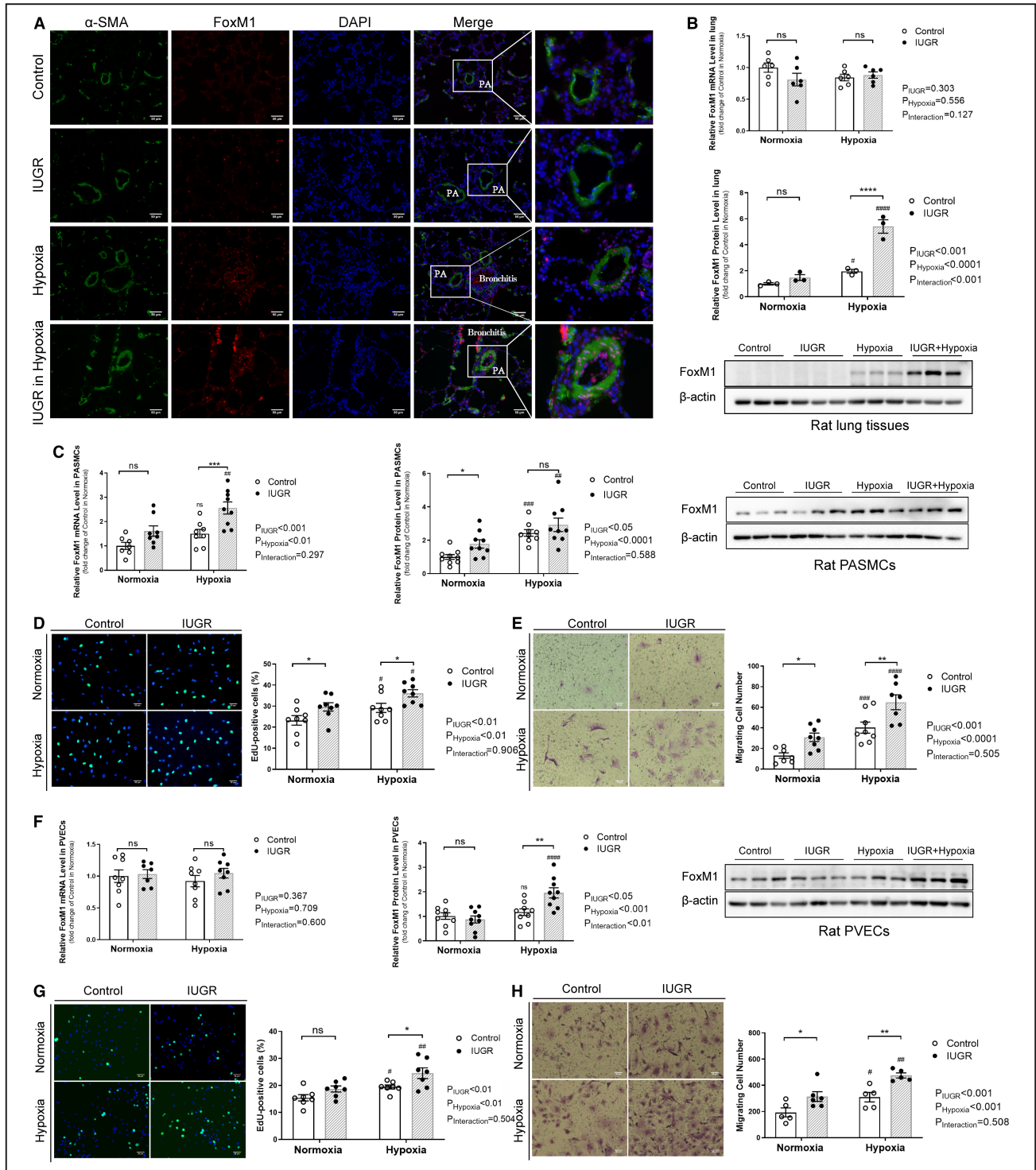
A, Representative immunofluorescence photomicrographs of α -smooth muscle actin (green) and FoxM1 (red) in small pulmonary arteries from rat lungs. Nuclei were counterstained with DAPI (blue). **B**, Relative mRNA expression ($n=6$ per group) and Western blot analysis ($n=3$ per group) of FoxM1 in lung tissues. **C**, Relative mRNA expression ($n=7-9$ per group) and Western blot analysis ($n=9$ per group) of FoxM1 in pulmonary arterial smooth muscle cells. **D**, Proliferation of pulmonary arterial smooth muscle cells ($n=8$ per group). **E**, Migration of pulmonary arterial smooth muscle cells ($n=7-8$ per group). **F**, Relative mRNA expression ($n=7-8$ per group) and Western blot analysis ($n=9$ per group) of FoxM1 in pulmonary vascular endothelial cells. **G**, Proliferation of pulmonary vascular endothelial cells ($n=7$ per group). **H**, Migration of pulmonary vascular endothelial cells ($n=5-6$ per group). All data were represented as the mean \pm SEM. Scale bar= $50\ \mu\text{m}$. Comparisons in B-E were made using 2-way ANOVA. α -SMA indicates α -smooth muscle actin; DAPI, 4',6'-diamidino-2-phenylindole; EdU, 5-ethynyl-2'-deoxyuridine; FoxM1, Forkhead box M1; IUGR, intrauterine growth restriction; PA, pulmonary artery; PASMCs, pulmonary arterial smooth muscle cells; and PVECs, pulmonary vascular endothelial cells. * $P<0.05$, ** $P<0.01$, *** $P<0.001$, **** $P<0.0001$, comparison between intrauterine growth restriction and control groups as indicated; # $P<0.05$, ## $P<0.01$, ### $P<0.001$, #### $P<0.0001$, comparison with relative group under normoxia.

(Figure 1E), and the muscularization of distal pulmonary vessels (Figure 1F), with the greatest augment in the IUGR group under the hypoxic condition.

FoxM1 Expression Was Remarkably Increased in IUGR-Induced PH

Immunofluorescence of FoxM1 in the lung showed that IUGR challenged with hypoxia expressed high

level of FoxM1 in vascular tissues (Figure 2A). Although there was no significant difference in the expression of FoxM1 in mRNA level, the protein level of FoxM1 was greatly augmented in lung tissues of the IUGR combined hypoxia group (Figure 2B). We next tested the expression of FoxM1 in the PASMCs and found that IUGR exaggerated the expression of FoxM1 in PASMCs, with more apparent increase after exposure to hypoxia (Figure 2C). 5-ethynyl-2'-deoxyuridine and



transwell assay showed that both the proliferation and migration of IUGR PSMCs were significantly augmented and greater elevations were found in hypoxic condition (Figure 2D and 2E). Similar phenomena were found in PVECs, which showed the significant elevations in FoxM1 expression, proliferation, and migration of IUGR PVECs, with more apparent increases after exposure to hypoxia (Figure 2F through 2H).

FoxM1 Played an Essential Role in the Crosstalk Between PVECs and PASMCs

Cocultured with PVECs from the control group, the abnormal expression of FoxM1 from the IUGR or hypoxia group was reversed in PASMCs (Figure 3A). The increases in proliferation and migration were diminished

as well (Figure 3B). While cocultured with PVECs from IUGR or hypoxia-exposed rats, FoxM1 expression of control PASMCs was augmented in the protein level (Figure 3C), in conjunction with the proliferation and migration, especially under the hypoxic condition (Figure 3D).

Exosomes Identification and Comparison of Exosomal miRNAs Signatures Between IUGR and Control Group

Both the proliferation and migration of control PASMCs were significantly exaggerated when PASMCs were cocultured with PVEC-derived medium of IUGR. (Figure S2A and S2B). To address how PVECs communicated with PASMCs, exosomes were extracted

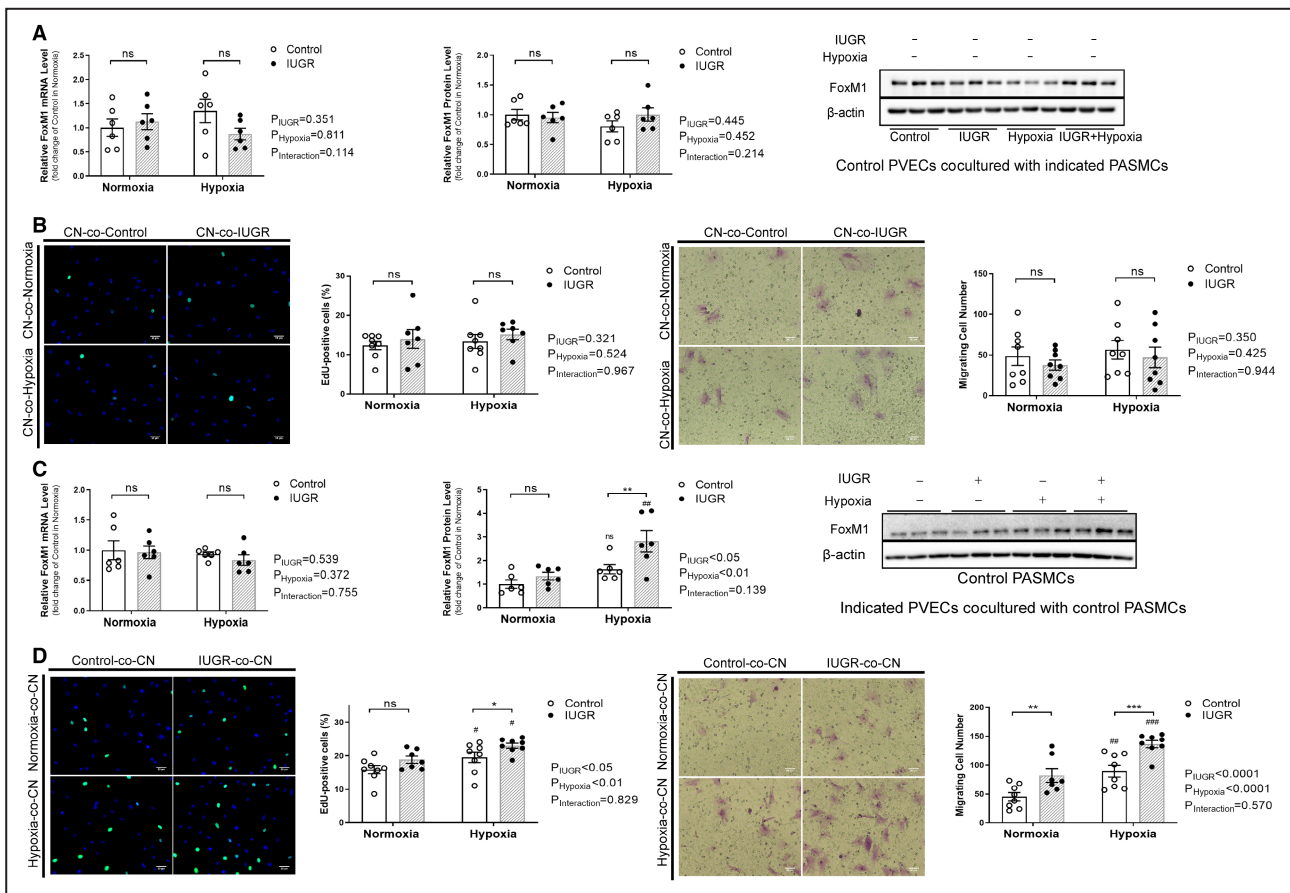


Figure 3. FoxM1 played an essential role in the crosstalk between PVECs and PASMCs.

A, Relative mRNA expression (n=6 per group) and Western blot analysis (n=6 per group) of FoxM1 in PASMCs isolated from intrauterine growth restriction or hypoxia-exposed rats after being cocultured with control PVECs. **B**, Proliferation (n=7–8 per group) and migration (n=8 per group) of PASMCs isolated from intrauterine growth restriction or hypoxia-exposed rats after being cocultured with control PVECs. **C**, Relative mRNA expression (n=6 per group) and Western blot analysis (n=6 per group) of FoxM1 in control PASMCs after being cocultured with PVECs from intrauterine growth restriction or hypoxia-exposed rats. **D**, Proliferation (n=7–8 per group) and migration (n=7–8 per group) of control PASMCs after being cocultured with PVECs from intrauterine growth restriction or hypoxia-exposed rats. All data were represented as the mean \pm SEM. Scale bar=50 μ m. Comparisons in **A** through **D** were made using 2-way ANOVA. co-CN indicates cocultured with control PASMCs; CN-co, control PVECs cocultured with; EdU, 5-ethynyl-2'-deoxyuridine; FoxM1, Forkhead box M1; IUGR, intrauterine growth restriction; PA, pulmonary artery; PASMCs, pulmonary arterial smooth muscle cells; and PVECs, pulmonary vascular endothelial cells. * $P<0.05$, ** $P<0.01$, *** $P<0.001$, comparison as indicated; # $P<0.05$, ## $P<0.01$, ### $P<0.001$, #### $P<0.0001$, comparison with coculture systems of relative normoxia-derived PVECs.

from PVEC-derived medium. The morphology of isolated exosomes was observed by transmission electron microscope, which showed typical cup shape and rounded lipid bilayer particles (Figure 4A). The size distribution of exosomes was evaluated by nanoparticle tracking analysis, which confirmed that most of the particles were ≈ 100 nm in diameter (Figure 4B). Detailed descriptions of the vesicles were shown in Table S2. Moreover, enrichment of the exosome markers CD63, TSG101, and HSP70 were all detected in the isolated exosomes enriched fraction samples by Western blot, while calnexin was absent (Figure 4C), indicating the successful isolation of purified exosomes from PVEC-derived medium.

The illumina HiSeq high-throughput technology was used to sequence 2 small RNA libraries, which were separated from exosomes of the IUGR or control group. Data showed that 33 miRNAs were up-regulated, while 26 miRNAs were downregulated in the IUGR group compared with the control group (Figure 4E). The mean expression levels of differentially expressed miRNAs were complemented in Table S3. The heatmap showed the differential expression genes between groups in a more visualized way and presented that the expression of exosomal miR-214-3p, miR-326-3p, and miR-125b-2-3p from PVEC-derived medium of IUGR was greatly decreased (Figure 4D). Kyoto Encyclopedia of Genes and Genomes pathway enrichment analysis showed that differentially expressed miRNA target genes acted in many physiological and pathological processes, including Hippo, MAPK, and Wnt signaling pathway (Figure 4F). The enrichment *P* values of Kyoto Encyclopedia of Genes and Genomes pathway enrichment analysis were complemented as Table S4 for reference.

Exosomal miRNAs Regulated the Functions of PASMCs Through Targeting FoxM1

A significant elevation in the expression of FoxM1 in the protein level was found when control PASMCs were treated with purified PVEC-derived exosomes of IUGR (Figure 5A). In silico analysis (www.targetscan.org) identified that from a total of 26 miRNAs that were significantly downregulated in PVEC-derived medium of IUGR, 3 miRNAs (miR-214-3p, miR-326-3p, and miR-125b-2-3p) were all predicted to target the FoxM1 3' untranslated region (UTR) (Figure 5B). Dual-Luciferase assay validated the predicted binding sites on the 3'UTR of FoxM1, which showed that the luciferase activity was significantly downregulated in the PASMCs transfected with the luciferase reporter plasmid in combination with the mimics of miR-214-3p, miR-326-3p, or miR-125b-2-3p, while mutations of the predicted binding sites abrogated the reduction induced

by the relative mimics, confirming the specific binding of miR-214-3p, miR-326-3p, and miR-125b-2-3p in FoxM1 (Figure 5C).

To verify the downregulation of exosomal miRNAs in the testing set, we performed quantitative real-time polymerase chain reaction and found that the expression of exosomal miR-214-3p, miR-326-3p, or miR-125b-2-3p secreted by PVECs in the IUGR group was significantly lower than those in the control group (Figure 5D). In addition, the expression of miR-214-3p and miR-326-3p was also greatly downregulated in the plasma-derived exosomes of IUGR (Figure 5E), indicating that the miRNAs enclosed in exosomes can be stable in the circulation system and might be of diagnostic value.

Next, we transfected PASMCs with relative miRNA inhibitors to investigate the effects of decreased miRNAs on FoxM1 expression and cellular functions. Although transduction with the inhibitors of the 3 miRNAs in normal PASMCs showed no significant elevation in the expression of FoxM1 in the mRNA level, the protein level was greatly augmented (Figure 5F). The proliferation and migration of PASMCs were greatly exaggerated as well (Figure 5G). On the contrary, transfected PASMCs with relative mimics of miR-214-3p, miR-326-3p, and miR-125b-2-3p revealed reductions of FoxM1 expression both in the mRNA and protein level (Figure S3A). The proliferation and migration of PASMCs were also greatly inhibited (Figure S3B). To see if the combination of 3 miRNA inhibitors or mimics exhibit much bigger effects, we transfected the PASMCs with combined 3 miRNA inhibitors or mimics, respectively. Interestingly, while single treatments had only partial effects, the combined treatments with 3 miRNA inhibitors or mimics were significantly more potent on the FoxM1 expression, proliferation, and migration of PASMCs (Figure S4).

FoxM1 Inhibition Blocked the PVECs-PASMCs Crosstalk and Inhibited the Severity of PH

Transfection of small interfering RNA targeting FoxM1 can effectively knock down the expression of FoxM1 in PASMCs (Figure 6A). Under FoxM1 targeted deletion, the dysfunctions of PASMCs observed in the hypoxia-IUGR group were greatly ameliorated, and the proliferation of transfected PASMCs was even lower than the healthy controls (Figure 6B). The effect of PVECs' cocultivation on control PASMCs was blocked when the transfected control PASMCs were cocultured with hypoxia-IUGR PVECs (Figure 6C).

Treatment with thiostrepton, which has been reported to be a FoxM1 inhibitor,³⁰ can inhibit the expression of FoxM1 effectively (Figure 6D) and reverse the dysfunctions of PASMCs observed in the

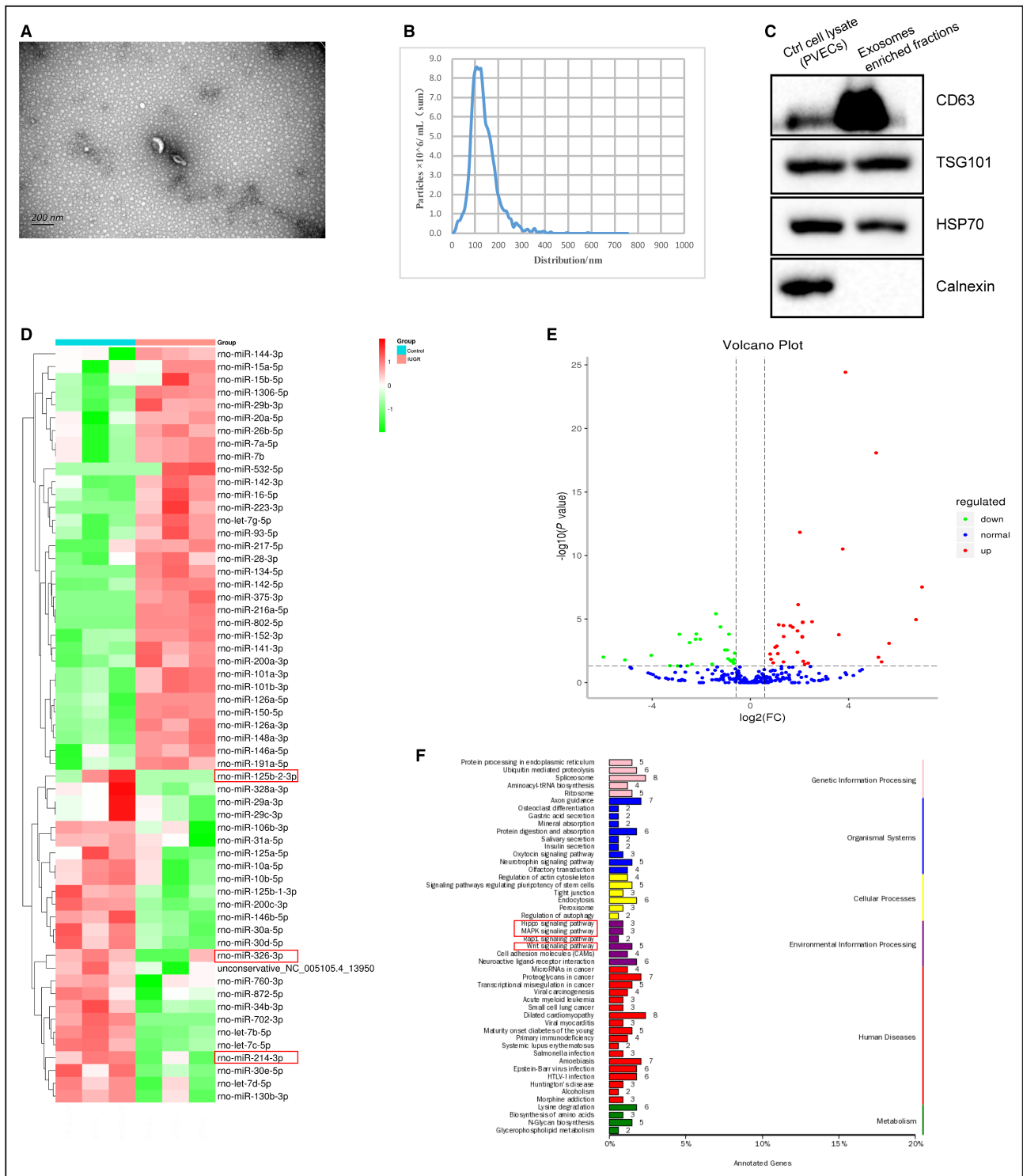


Figure 4. Exosomes identification and comparison of exosomal miRNAs signatures between the intrauterine growth restriction and control groups.

A, Representative transmission electron microscope picture of exosomes derived from pulmonary vascular endothelial cell-derived medium. Scale bar=200nm. **B**, The concentration and size distribution of the exosomes detected by nanoparticle tracking analysis. **C**, Western blot analysis for presence of exosomes markers, CD63, TSG101, and HSP70 and absence of calnexin. **D**, A heatmap of the expression level of 33 upregulated miRNAs and 26 downregulated miRNAs across all 6 samples in our exosomes enriched fractions miRNA data set. **E**, A volcano plot of the 59 differential expression genes. **F**, Kyoto Encyclopedia of Genes and Genomes pathway analysis of the differential exosomal miRNAs of intrauterine growth restriction. CD indicates clusters of differentiation; FC, fold change of control; HSP, heat shock protein; IUGR, intrauterine growth restriction; MAPK, mitogen-activated protein kinase; miR, microRNA; PVECs, pulmonary vascular endothelial cells; and TSG, tumor susceptibility gene.

hypoxia-IUGR group (Figure 6F). We also evaluated the therapeutic potential of thioestrepton in IUGR-induced PH rats in vivo. Treatment with thioestrepton significantly

ameliorated the elevated mPAP, RV hypertrophy index, vascular remodeling, and muscularization of distal pulmonary vessels in IUGR-induced PH rats (Figure 6G).

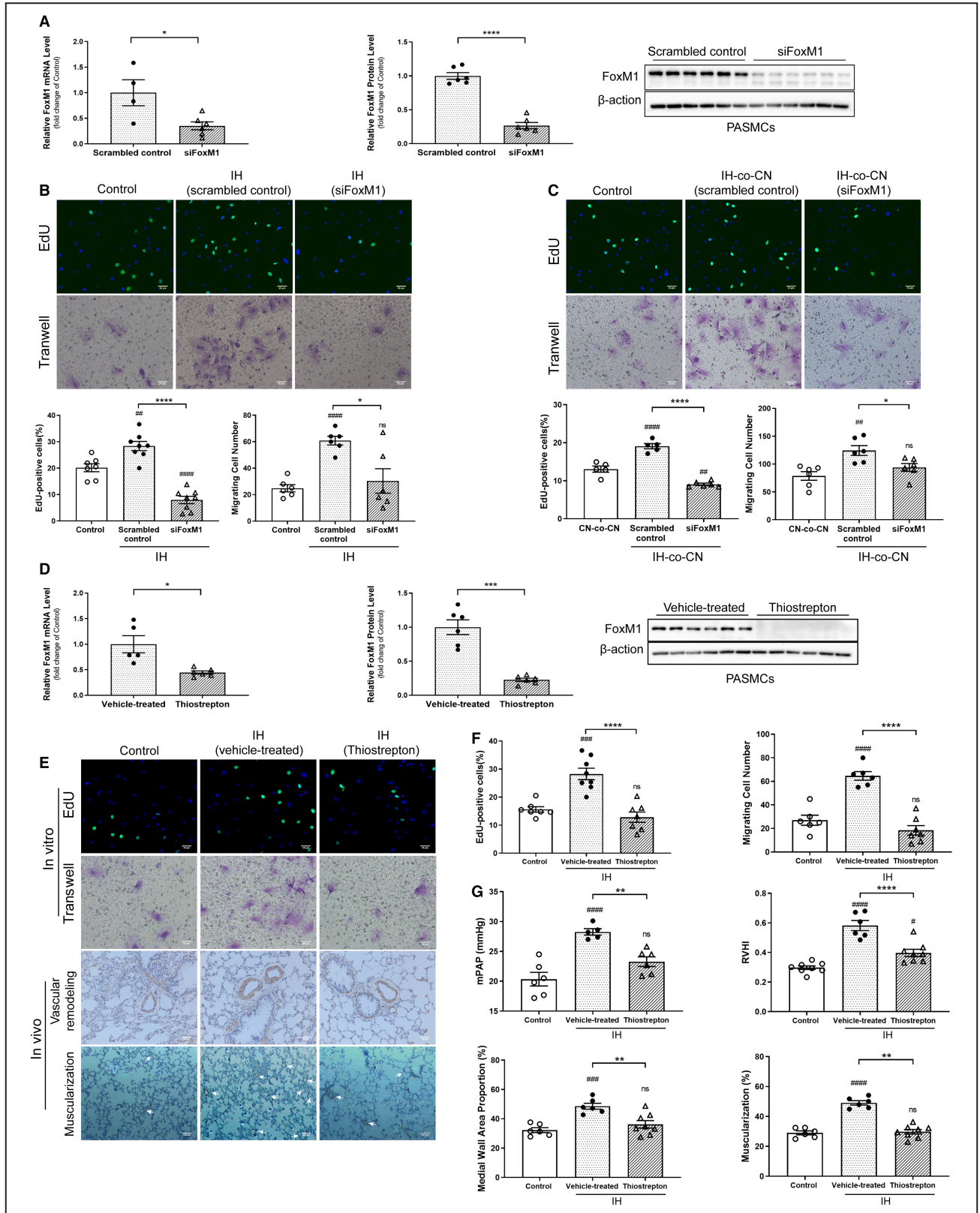


Figure 6. FoxM1 inhibition blocked the pulmonary vascular endothelial cells-PASMCs crosstalk and inhibited the severity of pulmonary hypertension.

A, Relative mRNA expression (n=4–6 per group, 48 hours) and Western blot analysis (n=6 per group, 72 hours) of FoxM1 in PASMCs transduced with FoxM1 small interfering RNA or scrambled small interfering RNA. **B**, Effects of FoxM1 small interfering RNA (72 hours) on the proliferation (n=7–8 per group) and migration (n=6 per group) of PASMCs. Scale bar=50 μm. **C**, Proliferation (n=5–6 per group) and migration (n=6 per group) of transfected control PASMCs (siFoxM1) after being cocultured with pulmonary vascular endothelial cells from hypoxia-exposed intrauterine growth restriction rats for 48 hours. CN indicates control. Scale bar=50 μm. **D**, Relative mRNA expression (n=5–6 per group, 16 hours) and Western blot analysis (n=6 per group, 24 hours) of FoxM1 in PASMCs treated with the FoxM1 inhibitor thiostrepton (4 μM) or dimethyl sulfoxide. **E**, Representative images of the proliferation and migration of PASMCs treated with thiostrepton (4 μM) in vitro, together with the vascular remodeling and muscularization of distal pulmonary vessels in thiostrepton-treated rats in vivo. Scale bar=50 μm in the first 3 figures and scale bar=100 μm in muscularization. **F**, Effects of thiostrepton (4 μM, 24 hours) on proliferation (n=7–8 per group) and migration (n=6–7 per group) of PASMCs. **G**, Mean pulmonary arterial pressure (n=5–6 per group), RV hypertrophy index (n=6–8 per group), medial wall area proportion of pulmonary arteriole (n=6–8 per group), and muscularization of distal pulmonary vessels (n=6–8 per group) in the hypoxia-exposed intrauterine growth restriction rats after treating with thiostrepton for 3 weeks. All data were represented as the mean±SEM. Comparisons in **A** and **D** were made using a Student *t*-test; comparisons in **B** (EdU), **C**, **F**, and **G** were made using 1-way ANOVA, and comparisons in **B** (transwell) were made using Welch ANOVA. CN-co-CN indicates control PVECs cocultured with control PASMCs; EdU, 5-ethynyl-2'-deoxyuridine; FoxM1, Forkhead box M1; IH, intrauterine growth restriction in hypoxia; IH-co-CN, IUGR-hypoxia PVECs cocultured with control PASMCs; mPAP, mean pulmonary arterial pressure; PASMCs, pulmonary arterial smooth muscle cells; RVHI, right ventricular hypertrophy index; and siFoxM1, small interfering Forkhead box M1. **P*<0.05, ***P*<0.01, ****P*<0.001, *****P*<0.0001, comparison as indicated; #*P*<0.05, ##*P*<0.01, ###*P*<0.001, ####*P*<0.0001, comparison with untreated controls.

Of note, although thiostrepton could greatly lower the RV hypertrophy index, the hypertrophic right ventricle could not return to normal.

DISCUSSION

Our results provided direct evidence that PASMCs were regulated by PVECs in a noncontact way. The exosomal miR-214-3p, miR-326-3p, and miR-125b-2-3p secreted by PVECs of IUGR were greatly downregulated, which was associated with overexpression of FoxM1, leading to hyperproliferation and excessive migration of PASMCs (Figure 7). Thus, FoxM1 may be a key regulator to mediate the crosstalk between PVECs and PASMCs and may be responsible for the IUGR-induced PH.

In line with the Developmental Origins of Health and Disease theory, the *Lancet* reported a stimulating discovery that young adults who suffered with adverse exposures during a critical fetal and perinatal period were predisposed to an augmented pulmonary arterial pressure increase at high altitude (4559m), although there was no significant difference at low altitude.⁷ In the present study, we induced IUGR in rats by nutrition restriction during pregnancy and found that all the pups' birth weights were below the 10th percentile of the controls. Further investigation found that the mPAP was similar in the 2 groups under normoxic conditions, while IUGR rats displayed a more significant increase in mPAP and more exaggerated pulmonary vascular remodeling compared with the controls after exposure to hypoxia. These results suggested that IUGR had a persistent effect on the pulmonary circulation that, when activated later in life, potentially developed into PH.

Prior studies identified the oncogenic role of FoxM1 in different cancers,³¹ and FoxM1 had been shown to regulate the proliferation of EC, SMC, and fibroblast in

different kinds of lung diseases.^{17,32–35} Recently, FoxM1 was reported to be involved in the endothelial autocrine pathway to mediate endothelial proliferation in the pathogenesis of PH.³⁶ Our studies demonstrated that FoxM1 was highly expressed in IUGR-induced PH that was associated with the hyperproliferation, as well as the excessive migration of PASMCs. Our findings prompted that the FoxM1 signaling may be one of the mechanisms that mediated pulmonary vascular remodeling and even IUGR-induced PH.

Emerging evidence suggested that pathologic crosstalk between PVECs and PASMCs may contribute to the disruption of vascular homeostasis. ECs acted as key regulators to PASMCs in 3 ways mostly, including contact-dependent signaling,²⁹ paracrine signaling,^{10,17} and signaling through extracellular vesicles.³⁷ We proved that the transfer of a signal occurred in a cell contact-independent manner between PVECs and PASMCs through a noncontact coculture system. Targeted deletion of FoxM1 in PASMCs blocked the PVECs-PASMCs crosstalk, indicating that PASMCs were probably regulated by PVECs via FoxM1 signaling. Intercepting the aberrant crosstalk between PVECs and PASMCs may be an effective way to prevent the development of IUGR-induced PH.

Exosomes have emerged as important transport vesicles to mediate intercellular communication. Exosomes can be integrated into the extracellular space when the multivesicular bodies fuse with the plasma membrane and are taken in by recipient cells through various processes, including direct fusion, endocytosis, or other specific recognitions.³⁸ Therefore, bioactive molecules contained in exosomes, such as proteins, lipids, and nucleic acids (mRNA, miRNAs, and DNA) were transferred to recipient cells.^{18,38} A recent study reported that extracellular vesicles were associated

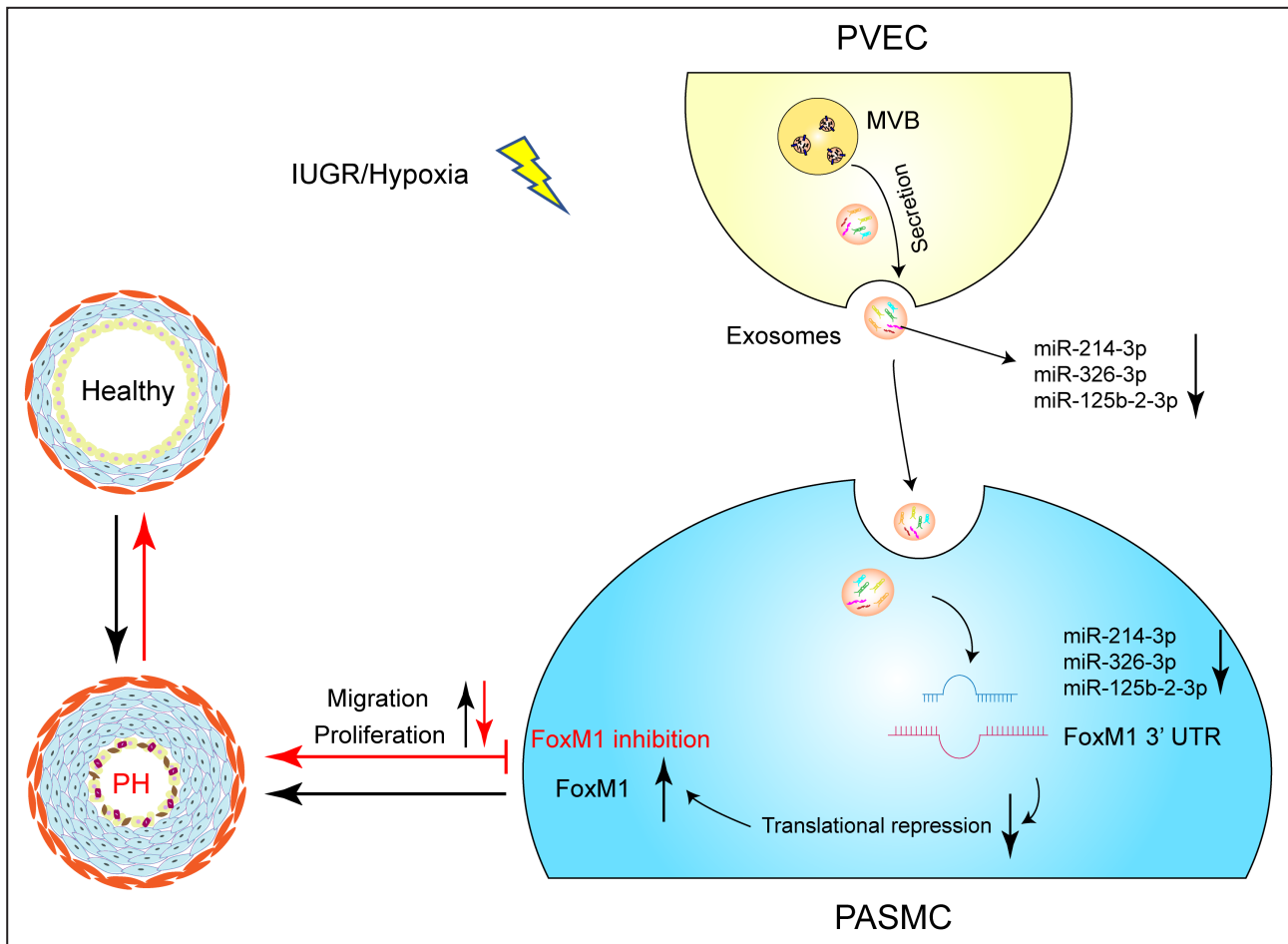


Figure 7. Pulmonary vascular endothelial cell-derived exosomal microRNAs regulate pulmonary arterial smooth muscle cells via FoxM1 (Forkhead box M1) signaling in intrauterine growth restriction-induced pulmonary hypertension.

FoxM1 indicates Forkhead box M1; IUGR, intrauterine growth restriction; miR, microRNA; MVB, multivesicular body; PASMC, pulmonary arterial smooth muscle cells; PH, pulmonary hypertension; and UTR, untranslated region.

with PH via modulation of tumor necrosis factor-beta signaling.³⁹ In the present study, we extracted vesicles from PVEC-derived medium and identified the purified exosomes through the typical morphology, original size, and specific exosome-associated molecules. We treated control PASMCs with purified PVEC-derived exosomes of IUGR and found that the FoxM1 expression in PASMCs was greatly upregulated. This result suggested that exosomes may be the vital mediators of PVECs-PASMCs crosstalk, which transferred signals from PVECs to PASMCs through FoxM1 signaling.

MiRNAs are major bioactive components of exosomes, that were reported to contribute to tumor aggressiveness and invasiveness.^{40,41} Our results uncovered that 33 miRNAs were upregulated, while 26 miRNAs were downregulated in PVEC-derived exosomes of IUGR. Those differentially expressed miRNA target genes acted in many vital processes. Hippo signaling pathway, MAPK signaling pathway, and Wnt signaling pathway were also involved, which were reported to

be associated with FoxM1 by a range of evidence.^{42–44} Commonly, miRNAs cannot catalyze any reactions by themselves, they form RNA induced silencing complexes and guide RNA induced silencing complexes to their targets in a sequence-specific manner, that negatively regulate their targets via post-transcriptional regulation predominantly.^{20,45} Our current findings demonstrated that miR-214-3p, miR-326-3p, and miR-125b-2-3p, which can specifically bind to the 3' UTR of FoxM1, were greatly downregulated in exosomes secreted by IUGR. As a result, the inhibited effect of RNA-induced silencing complexes on the translational repression of FoxM1 was decreased in PASMCs, which generated the over-expression of FoxM1 associated with the dysfunctions of PASMCs, promoting the IUGR-induced PH.

Studies have also proven that exosomes containing miRNAs derived from primary focus can be transferred into the body's circulation and serve as biomarkers for disease diagnosis and prognosis.^{18,46} Our current data uncovered that exosomal miR-214-3p and

miR-326-3p in plasma showed a similar decrease tendency in keeping with those in PVEC-derived medium, indicating the possibility of being biomarkers for clinical application. Further studies of the correlation between exosomal miRNAs and the severity of PH are needed.

Given that FoxM1 was overexpressed in IUGR-induced PH and served as a common target of miR-214-3p, miR-326-3p, and miR-125b-2-3p, FoxM1 inhibition could be an effective strategy for the treatment of this disease. Our study verified that genetic and pharmacological ablation of FoxM1 reversed the dysfunctions of PASMCs effectively. Treating IUGR-induced PH rats with FoxM1 inhibitor thioestrepton also remarkably attenuated PH features in vivo. Of note, thioestrepton treatment in rats could not absolutely reverse the RV hypertrophy, which was consistent with previous research.³³ A recent study found that pharmacological activation of bone morphogenetic protein signaling with FK506 (tacrolimus) improved RV function by decreasing RV afterload.⁴⁷ More extensive researches are warranted to investigate the combinations of drugs or other therapeutic modalities to ameliorate the pathologic changes of the myocardium.

In summary, we confirmed that undesirable perinatal environments left a persistent imprint in IUGR, making them highly sensitive to hypoxia later in life and potentially developed more significant PH. Our results provided clear evidence of PVECs-PASMCs crosstalk in the pathogenesis of IUGR-induced PH, which was mediated by exosomal miRNAs through targeting FoxM1. This study suggested a potential mechanism for the progression from IUGR to PH and might provide a novel therapeutic approach to treat this disease.

Our study had some limitations. Although we had demonstrated that IUGR decreased the exosomal miR-214-3p/miR-326-3p/miR-125b-2-3p to crosstalk with PASMCs through FoxM1 signaling, the means by which IUGR decreased the miRNAs enclosed in exosomes had not been uncovered. Furthermore, it was plausible that other pathways may participate in the pathophysiology of IUGR-induced PH. Whether FoxM1 can interact with other mechanisms should be investigated, which may help to inspire more desirable therapeutic strategies for IUGR-induced PH.

ARTICLE INFORMATION

Received June 15, 2022; accepted November 15, 2022.

Affiliations

Department of Neonatology, The Children's Hospital (X.L., C.H., Z.Z., Y.Y., Y.H., L.Y., Y.Z., L.D.); Department of Pediatric Health Care, The Children's Hospital (Y.L.); and Department of Rheumatology Immunology & Allergy, The Children's Hospital (X.X.), Zhejiang University School of Medicine, National Clinical Research Center for Child Health, Hangzhou, Zhejiang Province, People's Republic of China; (K.L.) and Department of Pediatrics, The First Affiliated Hospital, Zhejiang University School of Medicine, Hangzhou, Zhejiang Province, People's Republic of China (L.Y.).

Acknowledgments

We thank the Zhejiang Key Laboratory for Diagnosis and Therapy of Neonatal Diseases, Zhejiang Chinese Medical University Laboratory Animal Center and Key Laboratory of Reproductive Genetics, Ministry of Education, Zhejiang University. Study concept and design: All authors; Acquisition, analysis or interpretation of data: Luo, Hang, Le, Huang, and Ye; Statistical analysis: Zhang and Ying; Drafting of the manuscript: Luo and Hang; Critical revision of the manuscript for important intellectual content: All authors; Obtained funding: Zhong and Du; Administrative, technical, or material support: Zhang, Lv, Yan, and Xu; Study supervision: Xu, Zhong, and Du; Final approval of the version submitted for publication: All authors; Agreement to be accountable for all aspects of the work in ensuring that questions related to the accuracy or integrity of any part of the work are appropriately investigated and resolved: All authors.

Sources of Funding

This work was supported by grants from the National Natural Science Foundation of China (No. 81630037, 82001588).

Disclosures

None.

Supplemental Material

Data S1
Tables S1–S4
Figures S1–S4
References^{48–52}

REFERENCES

- Barker DJ. Fetal origins of coronary heart disease. *BMJ*. 1995;311:171–174. doi: 10.1136/bmj.311.6998.171
- Fetal Growth Restriction. ACOG practice bulletin, number 227. *Obstet Gynecol*. 2021;137:e16–e28.
- Barker DJ, Eriksson JG, Forsen T, Osmond C. Fetal origins of adult disease: strength of effects and biological basis. *Int J Epidemiol*. 2002;31:1235–1239. doi: 10.1093/ije/31.6.1235
- Lv Y, Fu L, Zhang Z, Gu W, Luo X, Zhong Y, Xu S, Wang Y, Yan L, Li M, et al. Increased expression of MicroRNA-206 inhibits potassium voltage-gated channel subfamily a member 5 in pulmonary arterial smooth muscle cells and is related to exaggerated pulmonary artery hypertension following intrauterine growth retardation in rats. *J Am Heart Assoc*. 2019;8:e010456. doi: 10.1161/JAHA.118.010456
- Hassoun PM. Pulmonary arterial hypertension. *N Engl J Med*. 2021;385:2361–2376. doi: 10.1056/NEJMra2000348
- Bhat R, Salas AA, Foster C, Carlo WA, Ambalavanan N. Prospective analysis of pulmonary hypertension in extremely low birth weight infants. *Pediatrics*. 2012;129:e682–e689. doi: 10.1542/peds.2011-1827
- Sartori C, Allemann Y, Trueb L, Delabays A, Nicod P, Scherrer U. Augmented vasoreactivity in adult life associated with perinatal vascular insult. *The Lancet*. 1999;353:2205–2207. doi: 10.1016/S0140-6736(98)08352-4
- Evans CE, Cober ND, Dai Z, Stewart DJ, Zhao YY. Endothelial cells in the pathogenesis of pulmonary arterial hypertension. *Eur Respir J*. 2021;58:2003957. doi: 10.1183/13993003.03957-2020
- Tajsc T, Morrell NW. Smooth muscle cell hypertrophy, proliferation, migration and apoptosis in pulmonary hypertension. *Compr Physiol*. 2011;1:295–317.
- Mercier O, Arthur A, Langer NB, Dorfmueller P, Lamrani L, Lecerf F, Decante B, Darteville P, Eddahibi S, Fadel E. Abnormal pulmonary endothelial cells may underlie the enigmatic pathogenesis of chronic thromboembolic pulmonary hypertension. *J Heart Lung Transplant*. 2017;36:305–314. doi: 10.1016/j.healun.2016.08.012
- Omura J, Satoh K, Kikuchi N, Satoh T, Kurosawa R, Nogi M, Otsuki T, Kozu K, Numano K, Suzuki K, et al. Protective roles of endothelial AMP-activated protein kinase against hypoxia-induced pulmonary hypertension in mice. *Circ Res*. 2016;119:197–209. doi: 10.1161/CIRCRESAHA.115.308178
- Gao Y, Chen T, Raj JU. Endothelial and smooth muscle cell interactions in the pathobiology of pulmonary hypertension. *Am J Respir Cell Mol Biol*. 2016;54:451–460. doi: 10.1165/rcmb.2015-0323TR
- Wierstra I. The transcription factor FOXM1 (Forkhead box M1): proliferation-specific expression, transcription factor function, target

- genes, mouse models, and normal biological roles. *Adv Cancer Res.* 2013;118:97–398. doi: [10.1016/B978-0-12-407173-5.00004-2](https://doi.org/10.1016/B978-0-12-407173-5.00004-2)
14. Costa RH. FoxM1 dances with mitosis. *Nat Cell Biol.* 2005;7:108–110. doi: [10.1038/ncb0205-108](https://doi.org/10.1038/ncb0205-108)
 15. Ustiyani V, Wang IC, Ren X, Zhang Y, Snyder J, Xu Y, Wert SE, Lessard JL, Kalin TV, Kalinichenko VV. Forkhead box M1 transcriptional factor is required for smooth muscle cells during embryonic development of blood vessels and esophagus. *Dev Biol.* 2009;336:266–279. doi: [10.1016/j.ydbio.2009.10.007](https://doi.org/10.1016/j.ydbio.2009.10.007)
 16. Lam EW, Brosens JJ, Gomes AR, Koo CY. Forkhead box proteins: tuning forks for transcriptional harmony. *Nat Rev Cancer.* 2013;13:482–495. doi: [10.1038/nrc3539](https://doi.org/10.1038/nrc3539)
 17. Dai Z, Zhu MM, Peng Y, Jin H, Machireddy N, Qian Z, Zhang X, Zhao YY. Endothelial and smooth muscle cell interaction via FoxM1 signaling mediates vascular remodeling and pulmonary hypertension. *Am J Respir Crit Care Med.* 2018;198:788–802. doi: [10.1164/rccm.201709-1835OC](https://doi.org/10.1164/rccm.201709-1835OC)
 18. Zhang L, Yu D. Exosomes in cancer development, metastasis, and immunity. *Biochim Biophys Acta Rev Cancer.* 2019;1871:455–468. doi: [10.1016/j.bbcan.2019.04.004](https://doi.org/10.1016/j.bbcan.2019.04.004)
 19. Yanez-Mo M, Siljander PR, Andreu Z, Zavec AB, Borrás FE, Buzas EI, Buzas K, Casal E, Cappello F, Carvalho J, et al. Biological properties of extracellular vesicles and their physiological functions. *J Extracell Vesicles.* 2015;4:27066. doi: [10.3402/jev.v4.27066](https://doi.org/10.3402/jev.v4.27066)
 20. Kawamata T, Tomari Y. Making RISC. *Trends Biochem Sci.* 2010;35:368–376. doi: [10.1016/j.tibs.2010.03.009](https://doi.org/10.1016/j.tibs.2010.03.009)
 21. Cheng L, Sharples RA, Scicluna BJ, Hill AF. Exosomes provide a protective and enriched source of miRNA for biomarker profiling compared to intracellular and cell-free blood. *J Extracell Vesicles.* 2014;3. doi: [10.3402/jev.v3.23743](https://doi.org/10.3402/jev.v3.23743)
 22. Zhou G, Chen T, Raj JU. MicroRNAs in pulmonary arterial hypertension. *Am J Respir Cell Mol Biol.* 2015;52:139–151. doi: [10.1165/rcmb.2014-0166TR](https://doi.org/10.1165/rcmb.2014-0166TR)
 23. Xu XF, Lv Y, Gu WZ, Tang LL, Wei JK, Zhang LY, Du LZ. Epigenetics of hypoxic pulmonary arterial hypertension following intrauterine growth retardation rat: epigenetics in PAH following IUGR. *Respir Res.* 2013;14:20. doi: [10.1186/1465-9921-14-20](https://doi.org/10.1186/1465-9921-14-20)
 24. Zhang Z, Luo X, Lv Y, Yan L, Xu S, Wang Y, Zhong Y, Hang C, Jyotsnav J, Lai D, et al. Intrauterine growth restriction programs intergenerational transmission of pulmonary arterial hypertension and endothelial dysfunction via sperm epigenetic modifications. *Hypertension.* 2019;74:1160–1171. doi: [10.1161/HYPERTENSIONAHA.119.13634](https://doi.org/10.1161/HYPERTENSIONAHA.119.13634)
 25. Davis GK, Newsome AD, Cole AB, Ojeda NB, Alexander BT. Chronic estrogen supplementation prevents the increase in blood pressure in female intrauterine growth-restricted offspring at 12 months of age. *Hypertension.* 2019;73:1128–1136. doi: [10.1161/HYPERTENSIONAHA.118.12379](https://doi.org/10.1161/HYPERTENSIONAHA.118.12379)
 26. Ojeda NB, Grigore D, Robertson EB, Alexander BT. Estrogen protects against increased blood pressure in postpubertal female growth restricted offspring. *Hypertension.* 2007;50:679–685. doi: [10.1161/HYPERTENSIONAHA.107.091785](https://doi.org/10.1161/HYPERTENSIONAHA.107.091785)
 27. Wang Y, Dai S, Cheng X, Prado E, Yan L, Hu J, He Q, Lv Y, Lv Y, Du L. Notch3 signaling activation in smooth muscle cells promotes extrauterine growth restriction-induced pulmonary hypertension. *Nutr Metab Cardiovasc Dis.* 2019;29:639–651. doi: [10.1016/j.numecd.2019.03.004](https://doi.org/10.1016/j.numecd.2019.03.004)
 28. Zhou J, Li YS, Nguyen P, Wang KC, Weiss A, Kuo YC, Chiu JJ, Shyy JY, Chien S. Regulation of vascular smooth muscle cell turnover by endothelial cell-secreted microRNA-126: role of shear stress. *Circ Res.* 2013;113:40–51. doi: [10.1161/CIRCRESAHA.113.280883](https://doi.org/10.1161/CIRCRESAHA.113.280883)
 29. Gairhe S, Bauer NN, Gebb SA, McMurtry IF. Serotonin passes through myoendothelial gap junctions to promote pulmonary arterial smooth muscle cell differentiation. *Am J Physiol Lung Cell Mol Physiol.* 2012;303:L767–L777. doi: [10.1152/ajplung.00183.2012](https://doi.org/10.1152/ajplung.00183.2012)
 30. Hegde NS, Sanders DA, Rodriguez R, Balasubramanian S. The transcription factor FOXM1 is a cellular target of the natural product thioestron. *Nat Chem.* 2011;3:725–731. doi: [10.1038/nchem.1114](https://doi.org/10.1038/nchem.1114)
 31. Nandi D, Cheema PS, Jaiswal N, Nag A. FoxM1: repurposing an oncogene as a biomarker. *Semin Cancer Biol.* 2018;52:74–84. doi: [10.1016/j.semcancer.2017.08.009](https://doi.org/10.1016/j.semcancer.2017.08.009)
 32. Huang X, Dai Z, Cai L, Sun K, Cho J, Albertine KH, Malik AB, Schraufnagel DE, Zhao YY. Endothelial p110gammaPI3K mediates endothelial regeneration and vascular repair after inflammatory vascular injury. *Circulation.* 2016;133:1093–1103.
 33. Bourgeois A, Lambert C, Habbout K, Ranchoux B, Paquet-Marceau S, Trinh I, Breuils-Bonnet S, Paradis R, Nadeau V, Paulin R, et al. FOXM1 promotes pulmonary artery smooth muscle cell expansion in pulmonary arterial hypertension. *J Mol Med (Berl).* 2018;96:223–235. doi: [10.1007/s00109-017-1619-0](https://doi.org/10.1007/s00109-017-1619-0)
 34. Penke LR, Speth JM, Dommeti VL, White ES, Bergin IL, Peters-Golden M. FOXM1 is a critical driver of lung fibroblast activation and fibrogenesis. *J Clin Invest.* 2018;128:2389–2405. doi: [10.1172/JCI87631](https://doi.org/10.1172/JCI87631)
 35. Zhao YY, Gao XP, Zhao YD, Mirza MK, Frey RS, Kalinichenko VV, Wang IC, Costa RH, Malik AB. Endothelial cell-restricted disruption of FoxM1 impairs endothelial repair following LPS-induced vascular injury. *J Clin Invest.* 2006;116:2333–2343. doi: [10.1172/JCI27154](https://doi.org/10.1172/JCI27154)
 36. Yi D, Liu B, Wang T, Liao Q, Zhu MM, Zhao YY, Dai Z. Endothelial autocrine signaling through CXCL12/CXCR4/FoxM1 axis contributes to severe pulmonary arterial hypertension. *Int J Mol Sci.* 2021;22:3182.
 37. Zhao L, Luo H, Li X, Li T, He J, Qi Q, Liu Y, Yu Z. Exosomes derived from human pulmonary artery endothelial cells shift the balance between proliferation and apoptosis of smooth muscle cells. *Cardiology.* 2017;137:43–53. doi: [10.1159/000453544](https://doi.org/10.1159/000453544)
 38. Xu R, Rai A, Chen M, Suwakulsiri W, Greening DW, Simpson RJ. Extracellular vesicles in cancer—implications for future improvements in cancer care. *Nat Rev Clin Oncol.* 2018;15:617–638. doi: [10.1038/s41571-018-0036-9](https://doi.org/10.1038/s41571-018-0036-9)
 39. Krishnamachary B, Mahajan A, Kumar A, Agarwal S, Mohan A, Chen L, Hsue PY, Chalise P, Morris A, Dhillon NK. Extracellular vesicle TGF-beta1 is linked to cardiopulmonary dysfunction in human immunodeficiency virus. *Am J Respir Cell Mol Biol.* 2021;65:413–429.
 40. Sun T, Kalionis B, Lv G, Xia S, Gao W. Role of exosomal noncoding RNAs in lung carcinogenesis. *Biomed Res Int.* 2015;2015:125807. doi: [10.1155/2015/125807](https://doi.org/10.1155/2015/125807)
 41. Yu F, Liang M, Huang Y, Wu W, Zheng B, Chen C. Hypoxic tumor-derived exosomal miR-31-5p promotes lung adenocarcinoma metastasis by negatively regulating SATB2-reversed EMT and activating MEK/ERK signaling. *J Exp Clin Cancer Res.* 2021;40:179. doi: [10.1186/s13046-021-01979-7](https://doi.org/10.1186/s13046-021-01979-7)
 42. Eisinger-Mathason TS, Mucaj V, Biju KM, Nakazawa MS, Gohil M, Cash TP, Yoon SS, Skuli N, Park KM, Gerech S, et al. Deregulation of the hippo pathway in soft-tissue sarcoma promotes FOXM1 expression and tumorigenesis. *Proc Natl Acad Sci USA.* 2015;112:E3402–E3411. doi: [10.1073/pnas.1420005112](https://doi.org/10.1073/pnas.1420005112)
 43. Goda C, Balli D, Black M, Milewski D, Le T, Ustiyani V, Ren X, Kalinichenko VV, Kalin TV. Loss of FOXM1 in macrophages promotes pulmonary fibrosis by activating p38 MAPK signaling pathway. *PLoS Genet.* 2020;16:e1008692. doi: [10.1371/journal.pgen.1008692](https://doi.org/10.1371/journal.pgen.1008692)
 44. Chen L, Xu Z, Li Q, Feng Q, Zheng C, Du Y, Yuan R, Peng X. USP28 facilitates pancreatic cancer progression through activation of Wnt/beta-catenin pathway via stabilising FOXM1. *Cell Death Dis.* 2021;12:887.
 45. He L, Hannon GJ. MicroRNAs: small RNAs with a big role in gene regulation. *Nat Rev Genet.* 2004;5:522–531. doi: [10.1038/nrg1379](https://doi.org/10.1038/nrg1379)
 46. Hannafon BN, Trigos YD, Calloway CL, Zhao YD, Lum DH, Welm AL, Zhao ZJ, Blick KE, Dooley WC, Ding WQ. Plasma exosome microRNAs are indicative of breast cancer. *Breast Cancer Res.* 2016;18:90. doi: [10.1186/s13058-016-0753-x](https://doi.org/10.1186/s13058-016-0753-x)
 47. Boehm M, Tian X, Ali MK, Mao Y, Ichimura K, Zhao M, Kuramoto K, Dannewitz Prosseda S, Fajardo G, Dufva MJ, et al. Improving right ventricular function by increasing BMP signaling with FK506. *Am J Respir Cell Mol Biol.* 2021;65:272–287. doi: [10.1165/rcmb.2020-0528OC](https://doi.org/10.1165/rcmb.2020-0528OC)
 48. Xia Y, Yang XR, Fu Z, Paudel O, Abramowitz J, Birnbaumer L and Sham JS. Classical transient receptor potential 1 and 6 contribute to hypoxic pulmonary hypertension through differential regulation of pulmonary vascular functions. *Hypertension.* 2014;63:173–80. doi: [10.1161/HYPERTENSIONAHA.113.01902](https://doi.org/10.1161/HYPERTENSIONAHA.113.01902)
 49. Sindi HA, Russomanno G, Satta S, Abdul-Salam VB, Jo KB, Qazi-Chaudhry B, Ainscough AJ, Szulcek R, Jan Bogaard H, Morgan CC, et al. Therapeutic potential of KLF2-induced exosomal microRNAs in pulmonary hypertension. *Nat Commun.* 2020;11:1185. doi: [10.1038/s41467-020-14966-x](https://doi.org/10.1038/s41467-020-14966-x)
 50. Ji H, Chen M, Greening DW, He W, Rai A, Zhang W, Simpson RJ. Deep sequencing of RNA from three different extracellular vesicle

-
- (EV) subtypes released from the human LIM1863 colon cancer cell line uncovers distinct miRNA-enrichment signatures. *PLoS One*. 2014;9:e110314. doi: [10.1371/journal.pone.0110314](https://doi.org/10.1371/journal.pone.0110314)
51. Min L, Zhu S, Chen L, Liu X, Wei R, Zhao L, Yang Y, Zhang Z, Kong G, Li P, et al. Evaluation of circulating small extracellular vesicles derived miRNAs as biomarkers of early colon cancer: a comparison with plasma total miRNAs. *J Extracell Vesicles*. 2019;8:1643670. doi: [10.1080/20013078.2019.1643670](https://doi.org/10.1080/20013078.2019.1643670)
52. Zhang Y, Chang X, Wu D, Deng M, Miao J, Jin Z. Down-regulation of Exosomal miR-214-3p targeting CCN2 contributes to endometriosis fibrosis and the role of exosomes in the horizontal transfer of miR-214-3p. *Reprod Sci*. 2021;28:715–727. doi: [10.1007/s43032-020-00350-z](https://doi.org/10.1007/s43032-020-00350-z)

Supplemental Material

Data S1.

Supplemental Methods

In vivo assessment of the mean pulmonary arterial pressure (mPAP), right ventricular (RV) hypertrophy, and pulmonary vascular remodeling

Before sacrifice, rats were anesthetized with 2% pentobarbital sodium (50 mg/kg, intraperitoneally). The mPAP was measured blindly by a PE-50 catheter, which was connected to a pressure transducer and inserted from the right jugular vein into the main pulmonary artery. A physiological data acquisition system (Biopac System, Inc) was used to identify the position of the catheter according to respective waveform. Blood was collected from the abdominal aorta using the anticoagulant tube containing EDTA for isolation of plasma. Then the heart was removed to assess the RV hypertrophy, using the formula: RVHI (right ventricular hypertrophy index) =right ventricular weight/ (left ventricular weight plus septum weight).

To assess the pulmonary vascular remodeling, rat lung tissues were harvested, fixed in 10% buffered formalin, embedded in paraffin, sectioned at 4-5 μm thickness, and stained with α -smooth muscle actin (α -SMA; CST, Cat #19245, 1:500). For each arteriole which was smaller than 100 μm in diameter, the proportion of the medial wall area (occupied by α -SMA) and the whole area (enclosed by blood vessel) were calculated to assess medial wall thickness, using Image J 1.8.0 (National Institutes of Health), respectively. The medial wall area proportion= (outer area – inner area)/outer area. All vessels of internal diameter <100 μm

were classified into nonmuscularized (<25 % α -SMA staining) and muscularized (\geq 25% α -SMA staining) vessels. Muscularization of distal pulmonary vessels were assessed by counting all muscularized vessels and expressed as a % of all (muscularized + non-muscularized) vessels^{48, 49}. Counting was performed by two blinded investigators. The mean of these measurements calculated was used as the representative value for each animal.

Immunofluorescent staining in lung

For immunofluorescent staining of FoxM1, rat lung sections were dewaxed and dehydrated, followed by boiling in 10 mmol/L sodium citrate (pH 6.0) for 10 min to retrieve antigen. Then, incubated the slides with monoclonal mouse anti-FoxM1 (Santa Cruz, Cat #sc-376471, 1:30) and monoclonal rabbit anti- α -SMA (CST, Cat #19245, 1:500) at 4°C overnight. Nuclei were counterstained with DAPI after a one-hour incubation with Alexa 594-conjugated goat anti-mouse secondary antibody (Abcam, Cat #ab150116, 1:1000) and Alexa 488-conjugated goat anti-rabbit secondary antibody (Abcam, Cat #ab150077, 1:1000) at room temperature. Images were taken using an optical microscope (Zeiss, Germany).

Immunofluorescence of PVECs and PASMCs

PVECs and PASMCs grown on chamber slides were fixed with 4% formaldehyde, permeabilized with 0.5% Triton and blocked with 3% BSA for 1 hour at room temperature. PVECs were incubated with specific cell marker CD31 (Abcam, Cat #ab24590, 1:30) and PASMCs were incubated with specific α -SMA (CST, Cat #19245, 1:500), respectively. Indirect immunofluorescence was conducted by incubation with Alexa 594-conjugated secondary antibodies (Abcam, goat anti-mouse Cat #ab150116, goat anti- rabbit Cat #ab150080; 1:1000). As a negative control, all slides were incubated with only secondary

antibody but with no primary to detect the background fluorescence (data not shown). After incubation, slides were counterstained with DAPI (for nuclear staining) and images were taken using an optical microscope (Zeiss, Germany).

Exosomes isolation and characterization

The exosomes were isolated from PVECs-derived medium using Total Exosome Isolation (from cell culture media) (Thermo Fisher Scientific, USA; Cat #4478359) according to the manufacturer's instructions. Briefly, exosome extraction reagent was added to the supernatant and incubated at 4°C overnight. Then centrifuged at 10000 g for 1h at 4°C to pellet the exosomes. Plasma was collected for exosomes isolation using Total Exosome Isolation (from plasma) (Thermo Fisher Scientific; Cat #4484451). Briefly, plasma was centrifuged at 2000g for 20 min to remove cells and debris. Centrifuged again at 10000g for 20 min to remove residual debris. Add proteinase K to the supernatant and incubated at 37°C for 10 min. Add exosome precipitation reagent and incubated at 2-8°C for 30min. Then centrifuged at 10000 g for 5min at room temperature to pellet the exosomes. The pellet was resuspended in PBS for further analyzed or stored at -80 °C.

For TEM studies, the exosomes were dropped onto the copper mesh and incubated at room temperature for 10 min. Then the copper mesh was contrasted by 2% uranyl acetate solution for 1 min and dried under an incandescent light for 2 min. Finally, the copper mesh was observed and photographed under a transmission electron microscope (H-7650, Hitachi Ltd., Tokyo, Japan). The size distribution and concentration of vesicle suspensions were detected by NTA using the ZetaView PMX 110 (Particle Metrix, Meerbusch, Germany) and the corresponding software ZetaView 8.02.28.

Small RNA library sequencing and differential expression analysis of miRNA

Two small RNA libraries (from exosomes isolated from PVECs-derived medium of control or IUGR rats) were constructed and sequenced on an Illumina HiSeq platform as previously reports^{50,51}. The differential miRNA expression analysis was performed using edgeR software. Hierarchical clustering analysis was performed to cluster the miRNAs with the same or similar expression behavior. Target gene prediction of selected miRNAs were performed using TargetScanHuman7.2. Kyoto Encyclopedia of Genes and Genomes (KEGG) pathway analysis was performed to generate further insights into potential signaling pathway related to these differentially expressed exosomal miRNAs.

Dual-Luciferase Assay

The rat FoxM1 promoter sequence (with or without the mutations in the predicted binding sites) was cloned into the pGL3-basic plasmid containing the sequence of a firefly luciferase as a reporter by Genomeditech (China). PSMCs were co-transfected with the plasmid (1ng/ul) and a vector contain a Renilla luciferase (0.1ng/ul, Promega) as an internal control, in combination with miR-214-3p, miR-326-3p and miR-125b-2-3p mimics or scrambled miRNA as control (both at 30 nmol/L, Sangon, China) using Lipofectamine 3000 transfection reagent (Thermo Fisher Scientific) according to manufacturer's instructions. After 48 hours, firefly and Renilla luciferase activities were measured using the Dual-Luciferase Reporter Assay System (Promega) by a luminometer (Infinite M1000 Pro, Tecan). Firefly luciferase activity(F) was normalized to Renilla luciferase activity(R) and luciferase activity was expressed as F/R and normalized to the scrambled miRNA group.

Treatments in PSMCs

PSMCs were made quiescent in serum-free medium for 24 h before treatments. Then incubated PSMCs with PVECs-derived medium or purified exosomes (10 $\mu\text{g/mL}$) in serum-free medium for 24h to verify the effects on PSMCs. For thioestrepton treatment, PSMCs were incubated with DMEM supplemented with 5% FBS in the absence or presence of thioestrepton (4 μM , TargetMol) after starvation treatment. The appropriate drug concentration was chosen according to the best inhibitory effect in our pre-experiments (data not shown).

Cell transfection

PSMCs or PVECs were transiently transfected using Lipofectamine RNAiMAX Transfection Reagent (Invitrogen) with small interfering RNA (siRNA) targeting FoxM1 (5'-GCAAUUUCCAGCUGGAAUTT-3') or control small interfering RNA (scramble siRNA; 5'-UUC UCC GAA CGU GUC ACG UTT-3'). The implication of miR-214-3p, miR-326-3p and miR-125b-2-3p were assessed using relative mimics or inhibitors (100nM, Sangon, China). For each experiment, we used a proper control (mimic or inhibitor negative control).

Cell Proliferation Assay

Cell proliferation was evaluated using EdU incorporation assay (Ribobio, China) according to the manufacturer's instructions. Briefly, cells were seeded equally into 96-well plates and cultured for another 48h with their own medium. Then cells were labeled with EdU for 2 h and incubated with 4% formaldehyde for 30 min. After that, cells were immunostained with related dye liquor for 30 min, then reacted with Hoechst 33342

reaction solution for 30 min to stain the nuclei. Finally, five random fields of each sample were imaged by an optical microscope (Zeiss, Germany) at 200× magnification. EdU-positive cells were expressed as a percentage of the numbers of EdU positive cells to the total number cells in each field. The average of the EdU-positive cells of the five fields was regarded as the value of the test.

Transwell Assay

A transwell assay was performed to assess the migration of PVECs or PASMCs using a 24-well transwell insert (8.0 μm; Coster) precoated with BD Matrigel matrix (BD Biosciences) as our previously study²⁴. Cells were resuspended in serum-free medium and added into the upper chamber, while the lower chamber was filled with medium supplemented with 5% FBS. After a 48-hour incubation, cells remained on the upper chamber were rubbed off, and the invaded cells on the lower surface of the membrane were fixed and stained with crystal violet (Beyotime, China). Six random microscopic fields were obtained using an optical microscope (Zeiss, Germany) and the total number of cells in the six fields were counted.

RNA Extraction, cDNA Synthesis, and QRT-PCR

Total RNA was extracted and purified from exosomes enriched fractions using SeraMir Exosome RNA Column Purification kit (System Biosciences, USA; Cat # RA808A-1) according to standard protocol. Total RNA of primary cells was isolated following the RNeasy protocol (Axygen, USA). Equal amounts of isolated RNA of primary cells were transcribed into cDNA using a reverse transcriptase kit (Takara, Japan), and exoRNAs were reverse transcribed using a miRNA reverse transcription kit from Ribobio Corporation Ltd

with RT Primers. Reverse transcription reaction was performed following manufacturer's recommendations. QRT-PCR analysis was performed on the StepOnePlus Real Time PCR System (Thermo Fisher Scientific) with TB-Green protocol (Takara, Japan) and data was analyzed using the $\Delta\Delta C_t$ method. U6 was chosen as an internal control for analysis in exoRNAs⁵², cyclophilin A was chosen as an internal control for analysis in PSMCs¹⁷, and β -actin was chosen as an internal control for analysis in PVECs²⁴. Primers used in this study were listed below:

FoxM1 RT-PCR primer (5' to 3'):

F: ACCAATATCCAGTGGCTTGG; R: GCTGTTGATCGCGAACTGTA

Cyclophilin A RT-PCR primer (5' to 3'):

F: TCAACCCACCGTGTCTTC; R: TCCTTTCTCCCCAGTGCTCA

β -actin RT-PCR primer (5' to 3'):

F: GCCAACCGTGAAAAGATG; R: TGCCAGTGGTACGACCAG

Western Immunoblotting

Cellular samples and the exosomes enriched supernatant were homogenized in RIPA buffer (Beyotime, China) and quantified by a BCA Protein Assay Kit (Beyotime, China). Equivalent amounts of protein were separated in 10% sodium dodecyl sulfate polyacrylamide gel (SDSPAGE) and transferred to polyvinylidene difluoride membranes (Millipore, USA). After blocking, membranes were probed with the following antibodies: anti-FoxM1 (Santa Cruz, Cat #sc-376471, 1:300), anti- β -actin(Sigma, Cat #A2228, 1:10000), anti-CD63 (Santa Cruz, Cat #sc-5275, 1:200), anti-TSG101 (Abcam, Cat #ab125011, 1:1000), anti-HSP70 (Abcam, Cat #ab181606, 1:1000) and anti-Calnexin (Proteintech, Cat #10427-2, 1:500) at

4°C overnight. This was followed by a one-hour incubation with horseradish peroxidase (HRP)-conjugated secondary antibodies at room temperature. The blots were detected by using G: BOX gel doc system (Syngene, Frederick, MD, USA), expression was quantified using Quantity One software (Media Cybernetics) and normalized to β -actin.

Table S1. Major Resources Table.**Animals (in vivo studies)**

Species	Vendor or Source	Background Strain	Sex	Persistent ID / URL
Rat	purchased from Zhejiang Chinese Medical University Laboratory Animal Center.	Sprague-Dawley Rats	F, M	

Antibodies

Target antigen	Vendor or Source	Catalog #	Working concentration	Lot # (preferred but not required)	Persistent ID / URL
α -smooth muscle actin	CST	19245	1:500 for immunohistochemistry and immunofluorescence		
FoxM1	Santa Cruz	sc-376471	1:30 for immunofluorescence; 1:300 for western blot (WB)		
β -actin	Sigma	A2228	1:10000 for WB		
CD63	Santa Cruz	sc-5275	1:200 for WB		
TSG101	Abcam	ab125011	1:1000 for WB		
HSP70	Abcam	ab181606	1:1000 for WB		
Calnexin	Proteintech	10427-2	1:500 for WB		

DNA/cDNA Clones

Clone Name	Sequence (5'-3')	Source / Repository	Persistent ID / URL
siRNA targeting FoxM1	GCAAAUUUCCAGCUGGAAUTT	Sangon, China	
scramble siRNA	UUC UCC GAA CGU GUC ACG UTT	Sangon, China	
miR-214-3p	ACAGCAGGCACAGACAGGCAG	Sangon, China	
inhibitor-214-3p	(mC)(mU)(mG)(mC)(mC)(mU)(mG) (mU)(mC)(mU)(mG) (mU)(mG)(mC)(mC)(mU)(mG)(mC) (mU)(mG)(mU)	Sangon, China	

miR-326-3p	CCUCUGGGCCCUUCCUCCAGU	Sangon, China	
inhibitor-326-3p	(mA)(mC)(mU)(mG)(mG)(mA)(mG) (mG)(mA)(mA)(mG) (mG)(mG)(mC)(mC)(mC)(mA)(mG) (mA)(mG)(mG)	Sangon, China	
miR-125b-2-3p	ACAAGUCAGGCUCUUGGGACC U	Sangon, China	
inhibitor-125b-2-3p	(mA)(mG)(mG)(mU)(mC)(mC)(mC) (mA)(mA)(mG)(mA) (mG)(mC)(mC)(mU)(mG)(mA)(mC) (mU)(mU)(mG)(mU)	Sangon, China	
mimics nc	UUGUACUACACAAAAGUACUG	Sangon, China	
inhibitor nc	(mC)(mA)(mG)(mU)(mA)(mC)(mU) (mU)(mU)(mU)(mG) (mU)(mG)(mU)(mA)(mG)(mU)(mA) (mC)(mA)(mA)	Sangon, China	
FoxM1 Forward primer	ACCAATATCCAGTGGCTTGG	Tsingke, China	
FoxM1 Reverse primer	GCTGTTGATCGCGAACTGTA	Tsingke, China	
Cyclophilin A Forward primer	TCAACCCACCGTGTCTTC	Tsingke, China	
Cyclophilin A Reverse primer	TCCTTTCTCCCCAGTGCTCA	Tsingke, China	
β -actin Forward primer	GCCAACCGTGAAAAGATG	Tsingke, China	
β -actin Reverse primer	TGCCAGTGGTACGACCAG	Tsingke, China	
PGL3-CMV-LUC-Rat_foxm1 WT	Listed as below	Genome ditech, China	
PGL3-CMV-LUC-Rat_foxm1(r no-miR-214-3p) MT	Listed as below	Genome ditech, China	
PGL3-CMV-LUC-Rat_foxm1(r no-miR-326-3p) MT	Listed as below	Genome ditech, China	
PGL3-CMV-LUC-Rat_foxm1(r no-miR-125b-2-3p) MT	Listed as below	Genome ditech, China	

PGL3-CMV-LUC-Rat_foxm1 WT:

CACTGCTGGGACCTATGCAAGCAATAGGATCTCCAGAGTCCTCCACTCCCTGCT
GGCAAGTGAAGTGGGTGTGACAGAGCCGTGAGGACCAGGAAATGCCACCCATT
AGTCACTGCTGCTCCTGGCAGGATAACCCTTGAAATGGTGTGAGTTCCCAAG
TTGTCCTGTAATTATAAATGTAGCCATATTCCCTTAGCTCTCATTATCCAGAGACTGC
CAGGATGGGTAGGGTGACAAGGGGTTGCATTAGCTTCTGCTTGTGGCCTTTGGGG
GCAGGACCTGCAGTTCAGCCTCTTCACACTGTGGGTTCTGCTGTAGGCTTCTAGA
CACACAGGTGTCCTTGCCAGGACCCACTTACTGCCCTTTCCTCACAGCTCCCCCT
GGTTCTAAGCCAGTGGTACTGCATGAAGAAATCCTGCGGCAAAGCCTATTGGCTCT
GGGTGTGTGGGGACGGGTGTGCCTGAAGCAAAGCATGGGTACTCACGTGAGTC
CTTTAGGTGTTTCTCTGATCGTGTTCCTCAATCATGCCAGGGAGTCTAGCATTGAGA
ACTCAGGCTGAGGCCTGAGGAGGAGGAGGAAGTGACCACTGACTTGCCTGGCTT
CCTTAGCTTGCACCTGAGTTTTGCAAAAAGCCAC

(red indicates predicted binding sites of miR-214-3p on FoxM1 3' UTR; orange indicates predicted binding sites miR-326-3p of on FoxM1 3' UTR; blue indicates predicted binding sites of miR-125b-2-3p on FoxM1 3' UTR)

PGL3-CMV-LUC-Rat_foxm1(rno-miR-214-3p) MT:

CACTGCTGGGACCTATGCAAGCAATAGGATCTCCAGAGTCCTCCACTCAAGTAG
TGCAAGTGAAGTGGGTGTGACAGAGCCGTGAGGACCAGGAAATGCCACCCATT
AGTCAAAGTAGTCTCCTGGCAGGATAACCCTTGAAATGGTGTGAGTTC...

PGL3-CMV-LUC-Rat_foxm1(rno-miR-326-3p) MT:

CACTGCTGGGACCTATGCAAGCAATAGGATCTAAACTCTTCCTCCACTCCCTGCTG
GCAAGTGAAGTGGGTGTGACAGAGCCGTGAGGACCAGGAAATGCCACCCATTA
GTCACCTGCTGCTCCTGGCAGGATAACCCTTGAAATGGTGTGAGTTCCCAAGTT
GTCCTGTAATTATAAATGTAGCCATATTCCCTTAGCTCTCATTATAACTCTCCTGCCA
GGATGGGTAGGGTGACA...

PGL3-CMV-LUC-Rat_foxm1(rno-miR-125b-2-3p) MT:

.....GCTGAGGCCTGAGGAGGAGGAGGAAGTGACCACGTCAGGTCCTGGCTT
CCTTAGCTTGCACCTGAGTTTTGCAAAAAGCCAC

Cultured Cells

Name	Vendor or Source	Sex (F, M, or unknown)	Persistent ID / URL
PVEC	primary culture	M	
PASMC	primary culture	M	

Table S2. The descriptions of the vesicles.

number of cultured PVECs	$1 \times 10^6 \times 8$ pools
total volume of PVECs-derived medium	5ml \times 8 pools
total volume of vesicles in PBS (μ l)	30
mean partical size (nm)	136.3
partical size of the main peak (nm)	114.8
percentage of the main peak (%)	97.3
concentration (particles/ml)	9.1×10^7
original concentration (particles/ml)	9.1×10^9

Table S3. The mean expression levels of differentially expressed miRNA (miRNA-seq data).

#ID	Control 1	Control 2	Control 3	IUGR 1	IUGR 2	IUGR 3	PValue	FDR	log2FC	regulated
miR-125b-2-3p	0	59.75	514.15	0	0	0	0.0098	0.0842	-5.9890	down
miR-702-3p	51.82	179.25	90.73	0	0	0	0.0165	0.1249	-5.1078	down
miR-214-3p	51.82	268.88	211.71	0	27.12	0	0.0071	0.0624	-4.0393	down
miR-130b-3p	129.55	59.75	120.98	0	27.12	0	0.0469	0.2670	-3.2843	down
unconservative_ NC_005105.4_1 3950	77.73	298.76	60.49	19.48	0	34.26	0.0485	0.2670	-2.9691	down
miR-125b-1-3p	673.64	268.88	302.44	77.91	27.12	68.53	0.0002	0.0026	-2.8918	down
miR-326-3p	103.64	328.63	90.73	0	0	102.79	0.0482	0.2670	-2.5711	down
miR-760-3p	518.19	717.02	332.69	0	189.85	137.06	0.0007	0.0087	-2.4776	down
miR-106b-3p	155.46	119.5	120.98	19.48	54.24	0	0.0371	0.2150	-2.3797	down
miR-31a-5p	570.01	537.76	907.33	272.67	162.73	0	0.0004	0.0049	-2.2342	down
miR-146b-5p	492.28	418.26	786.35	155.81	135.6	102.79	0.0002	0.0026	-2.2038	down
miR-34b-3p	492.28	806.64	393.18	97.38	189.85	171.32	0.0004	0.0049	-2.0433	down
miR-872-5p	362.73	328.63	181.47	38.95	162.73	137.06	0.0353	0.2125	-1.5567	down
miR-30d-5p	10363.77	6811.66	9103.56	4460.11	3390.11	3118.04	0.0000	0.0002	-1.4057	down
miR-30a-5p	11037.41	7200.05	9496.73	5083.36	4502.06	3597.74	0.0000	0.0009	-1.2202	down
miR-200c-3p	1528.66	1314.53	1300.51	798.54	678.02	753.81	0.0028	0.0282	-1.0359	down
miR-30e-5p	3627.32	2509.56	3478.1	1694.45	2115.43	1747.47	0.0028	0.0282	-0.9466	down
miR-328a-3p	2616.85	2479.68	4778.61	2006.08	1762.86	2124.38	0.0132	0.1073	-0.9103	down
let-7b-5p	152554.6 7	162703.1 5	144689.0 9	88890.62	90990.45	98612.3	0.0002	0.0026	-0.8736	down
let-7d-5p	1995.03	1613.29	1905.4	895.92	1573.01	993.66	0.0169	0.1251	-0.8301	down
miR-29a-3p	20675.72	21480.64	40678.68	22281.08	17899.76	14082.58	0.0209	0.1469	-0.7805	down
miR-29c-3p	20701.63	21689.77	40860.15	22378.47	18062.49	14356.69	0.0211	0.1469	-0.7736	down
miR-10a-5p	3368.22	3913.72	4082.99	3291.52	2061.18	2467.02	0.0274	0.1782	-0.6837	down
miR-10b-5p	3316.41	3913.72	4082.99	3291.52	2061.18	2467.02	0.0311	0.1908	-0.6775	down
miR-125a-5p	27360.35	39525.57	32845.39	29195.23	19743.98	20627.03	0.0150	0.1160	-0.6692	down
let-7c-5p	190045.6	191742.3 5	172574.4	125486.9 1	130885.2 2	138118.9	0.0049	0.0465	-0.6401	down
miR-191a-5p	7099.18	12577.68	11492.86	21151.45	21886.53	17714.58	0.0057	0.0513	0.8047	up
miR-26b-5p	3575.5	1493.79	2510.28	4830.17	5695.38	4557.14	0.0147	0.1160	0.8389	up
miR-28-3p	466.37	388.38	756.11	1188.06	1328.92	890.87	0.0280	0.1783	0.9268	up
miR-93-5p	2409.58	1643.16	2449.79	3914.77	6156.43	4557.14	0.0017	0.0182	1.0080	up
let-7g-5p	1373.2	836.52	1119.04	2317.7	3091.78	2432.76	0.0013	0.0150	1.0769	up
miR-146a-5p	544.1	1583.41	998.06	2531.94	2169.67	2809.66	0.0054	0.0498	1.1172	up
miR-16-5p	40470.52	30652.49	28006.29	61740.42	104171.1 9	78430.7	0.0000	0.0008	1.1526	up

miR-150-5p	1088.2	1284.66	756.11	2863.04	3064.66	2878.19	0.0000	0.0008	1.3447	up
miR-1306-5p	181.37	119.5	151.22	447.96	433.93	411.17	0.0238	0.1579	1.3453	up
miR-29b-3p	1010.47	597.51	937.58	3096.76	2034.06	2090.11	0.0002	0.0034	1.3549	up
miR-126a-5p	492.28	627.39	272.2	1577.59	1573.01	1610.42	0.0000	0.0008	1.6227	up
miR-142-3p	1269.56	478.01	514.15	2064.51	3661.31	2638.34	0.0000	0.0009	1.7253	up
miR-15b-5p	207.28	89.63	302.44	292.15	1545.89	753.81	0.0041	0.0403	1.9148	up
miR-200a-3p	155.46	209.13	302.44	1207.54	650.9	925.13	0.0001	0.0016	1.9168	up
miR-152-3p	285	567.64	574.64	1908.69	1898.46	2295.7	0.0000	0.0000	1.9431	up
miR-126a-3p	6373.72	7349.43	4627.39	28805.7	21642.44	31317.46	0.0000	0.0000	2.0147	up
miR-7b	362.73	29.88	120.98	720.63	813.63	1027.93	0.0002	0.0034	2.1116	up
miR-7a-5p	362.73	29.88	120.98	720.63	813.63	1027.93	0.0003	0.0036	2.1123	up
miR-101b-3p	181.37	239.01	120.98	584.29	1111.95	993.66	0.0000	0.0006	2.1290	up
miR-101a-3p	181.37	239.01	120.98	584.29	1111.95	993.66	0.0000	0.0006	2.1292	up
miR-144-3p	51.82	59.75	0	253.19	189.85	137.06	0.0212	0.1469	2.1520	up
miR-20a-5p	51.82	0	30.24	136.34	135.6	205.59	0.0367	0.2150	2.2114	up
miR-15a-5p	51.82	0	60.49	38.95	325.45	342.64	0.0297	0.1859	2.3507	up
miR-141-3p	77.73	149.38	120.98	973.82	542.42	685.28	0.0000	0.0006	2.5106	up
miR-217-5p	0	0	90.73	331.1	298.33	685.28	0.0002	0.0027	3.6003	up
miR-223-3p	1088.2	1015.77	1058.55	6485.67	33575.61	8120.61	0.0000	0.0000	3.7578	up
miR-148a-3p	1010.47	1553.54	695.62	13769.87	15133.43	23813.6	0.0000	0.0000	3.8713	up
miR-142-5p	25.91	29.88	90.73	1480.21	2251.03	2192.91	0.0000	0.0000	5.1194	up
miR-134-5p	0	0	0	97.38	216.97	68.53	0.0102	0.0851	5.2122	up
miR-532-5p	0	0	0	0	189.85	239.85	0.0236	0.1579	5.3411	up
miR-802-5p	0	0	0	155.81	162.73	205.59	0.0008	0.0095	5.6468	up
miR-375-3p	0	0	0	155.81	271.21	719.55	0.0000	0.0005	6.7427	up
miR-216a-5p	0	0	0	409.01	352.57	582.49	0.0000	0.0000	6.9884	up

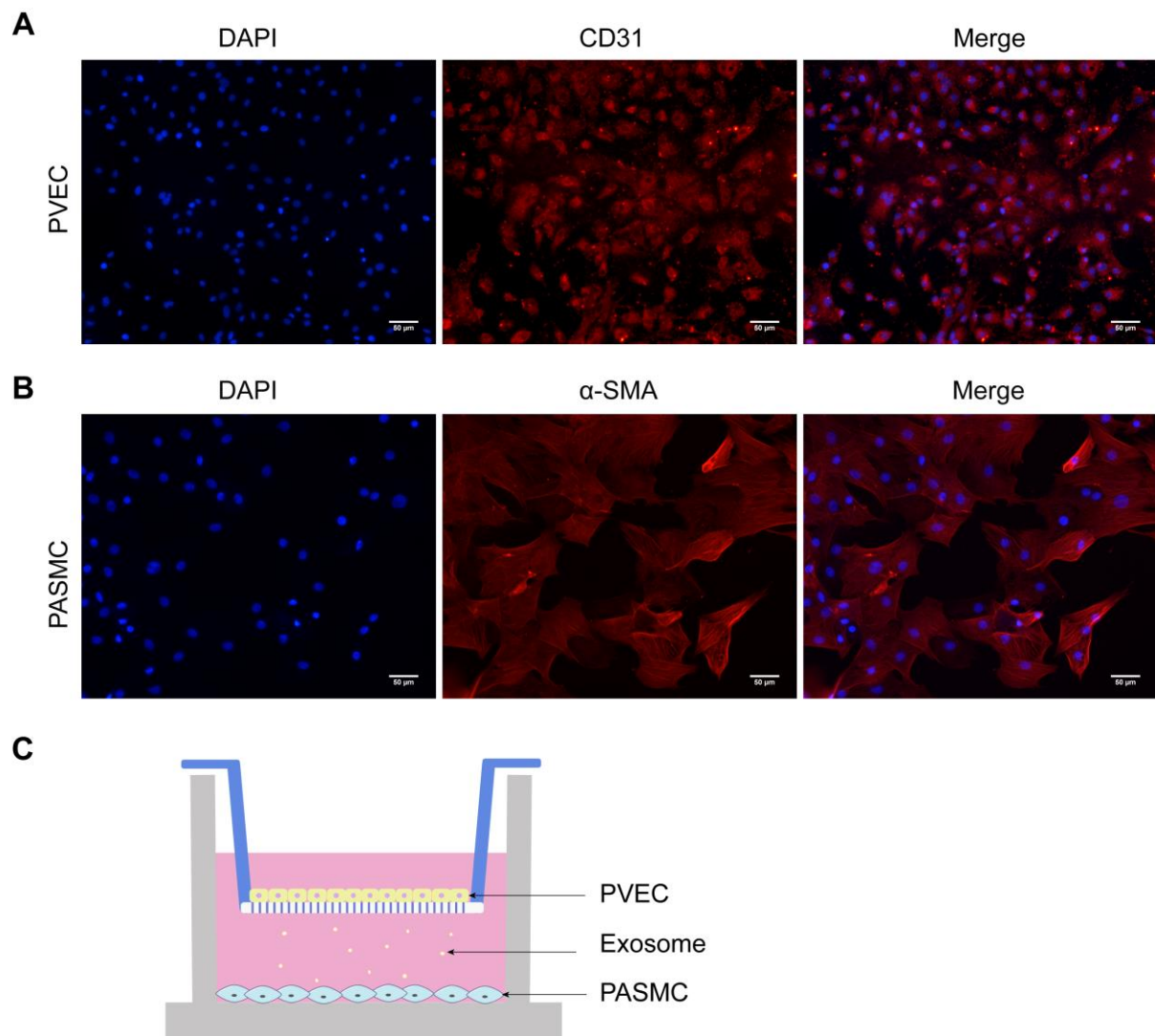
FDR indicates false discovery rate, FC indicates the fold change of Control.

Table S4. The enrichment p-values of KEGG pathway enrichment analysis.

KEGG pathway	P-value
Protein processing in endoplasmic reticulum	0.623790474
Ubiquitin mediated proteolysis	0.154450322
Spliceosome	0.008075758
Aminoacyl-tRNA biosynthesis	0.350302804
Ribosome	0.065213044
Axon guidance	0.292001706
Osteoclast differentiation	0.319004544
Gastric acid secretion	0.479065085
Mineral absorption	0.572257013
Protein digestion and absorption	0.19927067
Salivary secretion	0.205873332
Insulin secretion	0.262412729
Oxytocin signaling pathway	0.23833366
Neurotrophin signaling pathway	0.004392775
Olfactory transduction	0.940832062
Regulation of actin cytoskeleton	0.281462737
Signaling pathways regulating pluripotency of stem cells	0.121760309
Tight junction	0.82299247
Endocytosis	0.514873655
Peroxisome	0.686270222
Regulation of autophagy	0.205873332
Hippo signaling pathway	0.558522055
MAPK signaling pathway	0.23833366
Rap1 signaling pathway	0.374488887
Wnt signaling pathway	0.121760309
Cell adhesion molecules (CAMs)	0.58060671
Neuroactive ligand-receptor interaction	0.353870721
MicroRNAs in cancer	0.812194041
Proteoglycans in cancer	0.091963366
Transcriptional misregulation in cancer	0.715480741
Viral carcinogenesis	0.664086128
Acute myeloid leukemia	0.041131173
Small cell lung cancer	0.558522055
Dilated cardiomyopathy	0.306207536
Viral myocarditis	0.62611614
Maturity onset diabetes of the young	0.027544906
Primary immunodeficiency	0.078567877
Systemic lupus erythematosus	0.479065085
Salmonella infection	0.32116282
Amoebiasis	0.004028957

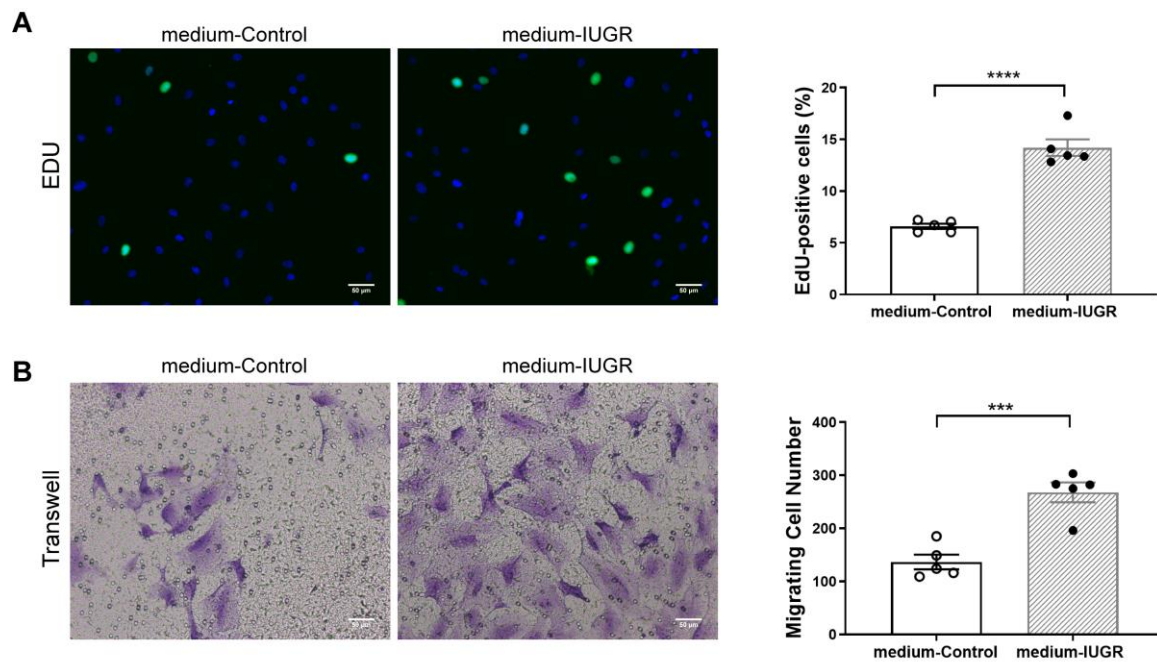
Epstein-Barr virus infection	0.273886491
HTLV-I infection	0.300148897
Huntington's disease	0.951560658
Alcoholism	0.572257013
Morphine addiction	0.404222108
Lysine degradation	0.012889368
Biosynthesis of amino acids	0.593225264
N-Glycan biosynthesis	0.019134527
Glycerophospholipid metabolism	0.6527525

Figure S1. PVECs/PASMCs identification and co-culture design.



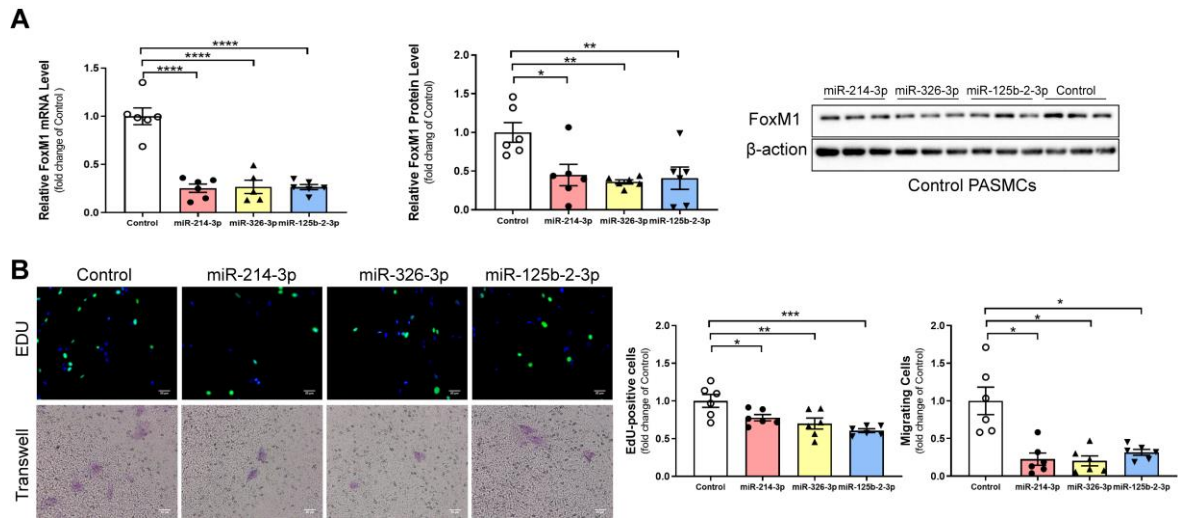
A, Detection of PVECs purity by specific cell marker CD31(red). B, Detection of PASMCs purity by specific α -smooth muscle actin (α -SMA, red). Nuclei were counterstained with DAPI (blue). Scale bars=50 μm . C, A model for the non-contact co-culture of PVECs and PASMCs.

Figure S2. Effects of PVECs-derived medium on control PSMCs.



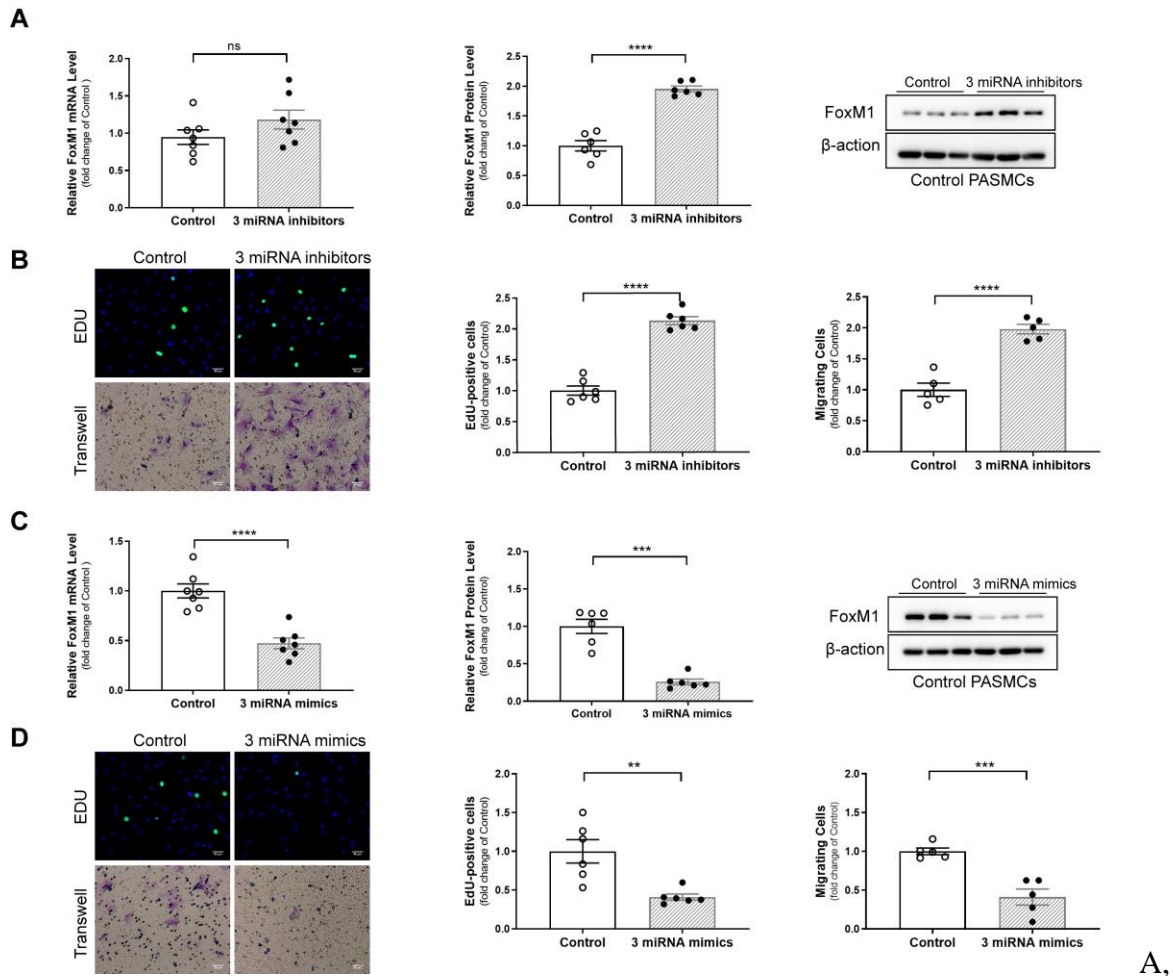
Proliferation (A) and migration (B) of control PSMCs after cocultured with PVECs-derived medium of control or IUGR. N=5 per group. All data were represented as the mean±SEM. Scale bars=50μm. Comparison in A was made using Student *t* test; comparisons in B was made using Mann-Whitney U test. *** $P<0.001$, **** $P<0.0001$, comparison between medium-IUGR and medium-Control groups as indicated.

Figure S3. Effects of miRNA mimics on control PAMSCs.



A, Relative mRNA expression (N=5-6 per group, 48h) and western blots analysis (N=6 per group, 72h) of FoxM1 in control PAMSCs transduced with miR-214-3p, miR-326-3p or miR-125b-2-3p mimics. B, Proliferation (N=6 per group) and migration (N=6 per group) of control PAMSCs transduced with miR-214-3p, miR-326-3p or miR-125b-2-3p mimics for 72h. All data were represented as the mean \pm SEM. Scar bar=50 μ m. Comparisons in A and B (EdU) were made using one-way ANOVA; comparisons in B (transwell) were made using Welch ANOVA. * P <0.05, ** P <0.01, *** P <0.001, **** P <0.0001, comparison with mimic negative controls as indicated.

Figure S4. Effects of combined treatment with 3 miRNA inhibitors or 3 miRNA mimics on control PSMCs.



Relative mRNA expression (N=7 per group, 48h) and western blots analysis (N=6 per group, 72h) of FoxM1 in control PSMCs transduced with 3 miRNA inhibitors. B, Proliferation (N=6 per group) and migration (N=5 per group) of control PSMCs transduced with 3 miRNA inhibitors for 72h. C, Relative mRNA expression (N=7 per group, 48h) and western blots analysis (N=6 per group, 72h) of FoxM1 in control PSMCs transduced with 3 miRNA mimics. D, Proliferation (N=6 per group) and migration (N=5 per group) of control PSMCs transduced with 3 miRNA mimics for 72h. All data were represented as the mean \pm SEM. Scar bar=50 μ m. All comparisons were made using Student *t* test. ** P <0.01, *** P <0.001, **** P <0.0001, comparison with controls as indicated.